HHS Public Access

Author manuscript

Mol Cell. Author manuscript; available in PMC 2022 March 04.

Published in final edited form as:

Mol Cell. 2021 March 04; 81(5): 1027–1042.e4. doi:10.1016/j.molcel.2020.12.030.

Alternative Lengthening of Telomeres is a Self-Perpetuating Process in ALT-Associated PML Bodies

Jia-Min Zhang[1], **Marie-Michelle Genois**[1], **Jian Ouyang**[1], **Li Lan**[1,2], **Lee Zou**[1,3,4]

[1]Massachusetts General Hospital Cancer Center, Harvard Medical School, Charlestown, MA 02129, USA

[2]Department of Radiation Oncology, Massachusetts General Hospital, Harvard Medical School, Boston, MA 02114, USA

[3]Department of Pathology, Massachusetts General Hospital, Harvard Medical School, Boston, MA 02114, USA

Abstract

Alternative lengthening of telomeres (ALT) is mediated by break-induced replication (BIR), but how BIR is regulated at telomeres is poorly understood. Here, we show that telomeric BIR is a self-perpetuating process. By tethering PML-IV to telomeres, we induced telomere clustering in ALT-associated PML bodies (APBs) and a POLD3-dependent ATR response at telomeres, showing that BIR generates replication stress. Ablation of BLM helicase activity in APBs abolishes telomere synthesis but causes multiple chromosome bridges between telomeres, revealing a function of BLM in processing inter-telomere BIR intermediates. Interestingly, the accumulation of BLM in APBs requires its own helicase activity and POLD3, suggesting that BIR triggers a feedforward loop to further recruit BLM. Enhancing BIR induces PIAS4-mediated TRF2 SUMOylation, and PIAS4 loss deprives APBs of repair proteins and compromises ALT telomere synthesis. Thus, a BLM-driven and PIAS4-mediated feedforward loop operates in APBs to perpetuate BIR, providing a critical mechanism to extend ALT telomeres.

eTOC Blurb

Alternative lengthening of telomere (ALT) occurs through break-induced replication (BIR) in ALT-associated PML bodies (APBs). Zhang et al. show that BLM promotes ALT by resolving BIR intermediates in APBs. Furthermore, BIR generates replication stress in APBs, driving a SUMO-mediated feedforward loop to further recruit BIR proteins and perpetuate ALT.

[4]Corresponding author: zou.lee@mgh.harvard.edu.
Lead contact: Lee Zou

Author contributions

J.-M.Z. and L.Z. designed the project. J.-M.Z., M.-M.G., J.O. and L.L. performed the experiments and data analysis. J.-M.Z. and L.Z. wrote the manuscript with help from all other authors.

Declaration of interests

All authors declare no competing interests. L.Z. is a member of the Advisory Board of Molecular Cell.

Graphical Abstract

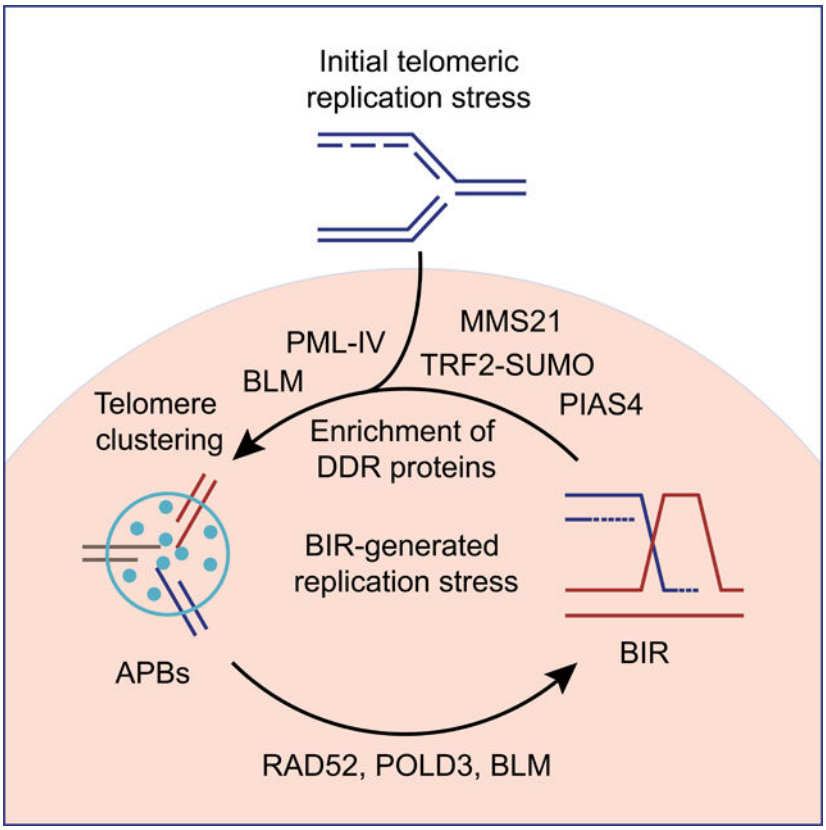

Introduction

Cancer cells have to maintain telomeres during proliferation to overcome replicative senescence and acquire immortality (Shay and Wright, 2019). While the majority of human cancers (>85%) uses telomerase to extend telomeres, a small but substantial fraction of human cancers (10–15%) relies on the alternative lengthening of telomere (ALT) pathway to overcome telomere shortening (Dilley and Greenberg, 2015; Hoang and O'Sullivan, 2020; Sobinoff and Pickett, 2020; Zhang and Zou, 2020). ALT activation is prevalent in certain cancer types, including sarcomas, glioblastoma, and neuroendocrine pancreatic cancer (Heaphy et al., 2011; Henson and Reddel, 2010). Because of its role in maintaining telomeres and suppressing genomic instability, the ALT pathway is an attractive target for cancer therapy (Flynn et al., 2015; Shay et al., 2012). Studies using model organisms suggest that ALT is mediated by DNA recombination and synthesis in telomere sequence (Chen et al., 2001; Neumann et al., 2013). Nevertheless, how the ATL pathway is activated in cancer cells and how this pathway operates at telomeres is still not fully understood.

Cumulative evidence suggests that DNA damage or replication stress at telomeres may be the trigger of ALT activation. Depletion of the histone chaperone ASF1 increases replication stress at telomeres and induces a number of ALT features (O'Sullivan et al., 2014). Generation of DNA double-stranded breaks (DSBs) in telomeres by the FokI nuclease fused

to TRF1 induces robust telomere synthesis, which resembles ALT (Dilley et al., 2016). In ALT-positive (ALT^+) cells, loss of FANCM, a DNA translocase that interacts with the BLM-TOP3A-RMI (BTR) complex and suppresses telomeric R-loops, increases replication stress at telomeres and enhances ALT features (Lu et al., 2019; Silva et al., 2019). Paradoxically, FANCM loss also reduces the viability of ALT^+ cells, suggesting that ALT^+ cells cannot tolerate excessive replication stress (Lu et al., 2019; Pan et al., 2017; Silva et al., 2019). The intrinsic replication stress at ALT telomeres may arise from multiple sources, such as telomeric R-loops and G quadruplexes (Amato et al., 2020; Arora et al., 2014). Notably, these sources of replication stress are not unique to ALT telomeres. Although ALT^+ cells may have higher telomere replication stress than ALT^- cells, it is still unclear what determines the threshold of replication stress to activate the ALT pathway. Furthermore, ALT is primarily active in G2 and M phases of the cell cycle (Min et al., 2017; Zhang et al., 2019), raising an important question as to what promotes ALT activation during these cell-cycle windows.

Once activated, the ALT pathway drives telomere DNA synthesis in ALT-associated PML bodies (APBs) in G2 cells or APB-like foci in mitotic cells (Cesare et al., 2009; Grobelny et al., 2000; Min et al., 2019; Yeager et al., 1999; Zhang et al., 2019). ALT telomere synthesis is a process of conservative DNA replication that requires POLD3 and POLD4, two accessary subunits of DNA polymerase δ important for break-induced DNA replication (BIR) (Dilley et al., 2016; Roumelioti et al., 2016). We and others showed that ALT is in fact a bifurcated BIR pathway operating through both RAD52-dependent and -independent mechanisms (Verma et al., 2019; Zhang et al., 2019). Loss of RAD52 or its interacting protein RAD51AP1 compromises ALT activity (Barroso-Gonzalez et al., 2019; Verma et al., 2019; Zhang et al., 2019). Depletion of PML, a key component of APBs, eliminates APBs and ALT telomere synthesis (Loe et al., 2020; Zhang et al., 2019). Loss of the BLM helicase also abolishes APBs and ALT telomere synthesis (Zhang et al., 2019), whereas overexpression of BLM enhances APBs and telomere extension (Min et al., 2019; Sobinoff et al., 2017). Remarkably, tethering of a poly(SUMO)-poly(SUMO-interacting motif) (SIM) fusion protein to telomeres in ALT^- cells is sufficient to induce APB-like condensates, and overexpression of BLM functionally activates ALT in these cells (Min et al., 2019). Furthermore, tethering of RMI1, a component of the BTR complex, to telomeres in PML knockout (KO) cells restores ALT activity, suggesting that the critical function of PML in ALT is to recruit BTR to telomeres (Loe et al., 2020). All these findings highlight that BLM is a key driver of ALT, focusing much attention on another important question: How does BLM drive ALT telomere synthesis in APBs?

In this study, we developed a conditional system to tether PML-IV to telomeres and induce APBs. Using this system, we found that the accumulation of PML-IV at telomeres is sufficient to promote SUMO-mediated telomere clustering in both ALT^+ and ALT^- cells. However, tethered PML-IV only stimulates telomere synthesis in ALT^+ cells, suggesting that APB formation is not sufficient to activate ALT. Importantly, this inducible system allowed us to bypass the function of BLM in APB formation and directly interrogate its roles in BIR. In cells harboring PML-IV-induced APBs, loss of BLM helicase activity resulted in a drastic increase of telomeric anaphase bridges in mitosis, showing that BLM is important for resolving BIR intermediates. Surprisingly, by inducing APBs and ALT activity, we found

that telomeric BIR itself generates replication stress. Ablation of BLM helicase activity or POLD3 reduced replication stress and the accumulation of BLM and RAD52 in APBs, suggesting that BIR triggers a feedforward loop to recruit DNA damage response (DDR) proteins. Furthermore, BIR stimulates the SUMOylation of TRF2 by PIAS4, and PIAS4 is required for the efficient accumulation of DDR proteins in APBs and ALT telomere synthesis. Together, these results reveal that telomeric BIR is a source of replication stress, which drives a PIAS4-mediated feedforward loop to recruit DDR proteins to APBs and promote further telomere synthesis. In addition, BLM drives ALT not only by promoting APB formation but also by processing BIR intermediates. These findings suggest that ALT is a self-perpetuating process enabled by APBs, shedding light on how replication stress triggers ALT in G2 and how BLM functions in BIR to extend telomeres.

Results

PML-IV is the main PML variant supporting ALT

We recently reported that ALT telomere synthesis occurs exclusively in APBs in G2 cells, and that depletion of PML abolishes ALT activity (Zhang et al., 2019). To understand how PML promotes ALT, we sought to recapitulate APB formation by tethering PML to telomeres. A previous study showed that tethering of PML-III, one of the six PML splicing variants, to the *lacO* repeats integrated to three subtelomeric loci induced *de novo* APB formation at adjacent telomeres (Chung et al., 2011). However, this approach did not recapitulate the clustering of telomeres in APBs, a key feature of ALT$^+$ cells (Draskovic et al., 2009; Min and Shay, 2019). Furthermore, the binding of the LacI repressor to *lacO* repeats blocks replication forks *in vitro* (Zhang et al., 2015), and integration of *lacO* repeats to a chromosome generates a fragile site in mammalian cells (Jacome and Fernandez-Capetillo, 2011), raising the possibility that LacI-mediated tethering of PML-III to the *lacO* repeats at subtelomeric loci induces APBs at least in part by generating replication stress. To investigate the effects of APB formation on telomeres without using *lacO* repeats, we sought to tether PML to endogenous telomeric repeats in an inducible manner.

Six splicing variants of PML, namely PML-I to -VI, are present in human cells (Jensen et al., 2001). To determine which of the PML variants can support ALT, we knocked out PML in the ALT$^+$ osteosarcoma cell line U2OS with CRISPR/Cas9, generating a U2OS-derivative line lacking all PML variants (Fig. S1A). Then, we individually expressed all six PML variants in PML KO cells (Fig. S1A), and analyzed the DNA synthesis at telomeres in synchronized G2 cells by EdU labeling and telomere fluorescence *in situ* hybridization (FISH) (Fig. S1B). Compared with wild-type cells, the telomere synthesis in PML KO cells was severely compromised. Among the PML variants, only PML-IV restored telomere synthesis to the wild-type level. PML KO cells also displayed an increased number of telomere foci compared with wild-type cells (Fig. S1C), indicating that telomere clustering was compromised. PML-IV was the only PML variant that restored telomere clustering to the wild-type level. The intensity of telomere FISH signals in PML KO cells was decreased compared to wild-type cells (Fig. S1D), indicating a reduction in telomere clustering and synthesis, and/or loss of telomeric DNA. Again, PML-IV was the only PML variant that

significantly increased telomere intensity in PML KO cells. Together, these results suggest that PML-IV is the main PML variant that functionally supports ALT.

Tethering of PML-IV to telomeres induces APBs and telomere clustering

To tether PML-IV to telomeres, we sought to induce an interaction between PML-IV and TRF1, a shelterin component binding to telomeric repeats directly. The plant abscisic acid (ABA) induces an interaction between the pyrabactin resistance-like protein (PYL1) and the ABA insensitive protein (ABI) (Liang et al., 2011). We fused PYL1 and TagRFP to TRF1, generating PYL1-TagRFP-TRF1 (Fig. 1A, referred to as $TRF1^{RFP}$). In addition, we fused ABI and EGFP to PML-IV, generating ABI-EGFP-PML-IV (Fig. 1A, referred to as PML-IV^{GFP}). In the following experiments, we co-expressed $TRF1^{RFP}$ with PML-IV^{GFP}, or with other forms of PML^{GFP} in cells. These pairs of fusion proteins allowed us to simultaneously follow the localizations of TRF1 and PML in cells, and to bring them together with ABA in an inducible manner.

In cells expressing both $TRF1^{RFP}$ and PML-IV^{GFP}, foci of both proteins were readily detected in the absence of ABA, but they did not colocalize (Fig. 1B). Upon ABA treatment, $TRF1^{RFP}$ and PML-IV^{GFP} became perfectly colocalized (Fig. 1B), showing a robust induction of APBs. Notably, the intensity of $TRF1^{RFP}$ foci was drastically increased by ABA (Fig. 1B), possibly owing to the clustering of telomeres and telomere synthesis (see below). The intensity of PML-IV^{GFP} foci was also increased by ABA (Fig. 1B), indicating the efficient accumulation of PML-IV at telomeres. In addition, ABA induced the colocalization of endogenous SP100 with telomeres (Fig. S1E), showing that PML bodies are indeed formed at telomeres. These results demonstrate that tethering of PML-IV to telomeres induces APBs robustly.

APB formation is dependent on protein SUMOylation (Potts and Yu, 2007). Moreover, PML can oligomerize through multivalent SUMO-SIM interactions, conferring phase-separating properties (Banani et al., 2016). To test whether the SUMO-SIM-mediated interactions of PML-IV are important for APB induction, we analyzed the PML-IV-3MAS mutant, which lacks all SUMOylation sites and SIMs (Fig. 1B) (Shen et al., 2006). In contrast to wild-type PML-IV^{GFP}, PML-IV-$3MAS^{GFP}$ formed aberrant aggregates in the absence of ABA (Fig. 1B). Upon ABA treatment, PML-IV-$3MAS^{GFP}$ and $TRF1^{RFP}$ colocalized at small foci, but the intensities of both proteins in these foci were much lower than in the APBs formed by wild-type PML-IV^{GFP}. These results show that PML-IV relies on the SUMO-SIM-mediated interactions to induce APBs efficiently.

To test whether tethering of PML-IV induces telomere clustering, we analyzed the number of telomere foci and telomere FISH intensity over time after ABA treatment. In cells expressing wild-type PML-IV^{GFP}, telomere number gradually declined, whereas telomere intensity gradually increased (Fig. 1C). In contrast, neither telomere number nor telomere intensity changed significantly in cells expressing PML-IV-$3MAS^{GFP}$ (Fig. 1C). To directly visualize telomere clustering, we performed time-lapse imaging of live cells expressing $TRF1^{RFP}$ and PML-IV^{GFP} after ABA treatment (Fig. 1D). Fusions between individual $TRF1^{RFP}$ foci were readily detectable after 10 hours of ABA exposure, providing direct evidence for telomere clustering. Next, we asked whether PML-IV induces telomere

clustering in ALT⁻ cells. TRF1^{RFP} and PML-IV^{GFP} were expressed in the ALT⁻ glioma cell line U-251 MG and the ALT⁻ untransformed retinal pigment epithelial cell line RPE1. ABA reduced the number of telomere foci but increased telomere intensity in these ALT⁻ cell lines (Fig. S1F–G), suggesting that tethering of PML-IV to telomeres induces telomere clustering in both ALT$^+$ and ALT⁻ cells.

Induction of APBs stimulates ALT activity

To evaluate the functional impacts of PML-IV on telomeres, we analyzed the localization of DDR proteins to APBs after ABA treatment. A number of DDR proteins implicated in BIR, including BLM, RAD52, MRE11 and PCNA, were increasingly colocalized with telomeres in U2OS cells after ABA exposure (Fig. 1E, S2A). Furthermore, telomere DNA synthesis was enhanced by ABA in U2OS cells expressing wild-type PML-IV^{GFP}, but the increase was diminished in cells expressing PML-IV-3MAS^{GFP} (Fig. 1F, S2B). These results suggest that the PML-IV-driven and SUMO-SIM-mediated APB formation stimulates recruitment of DDR proteins and telomere synthesis. Consistent with the idea that the telomere synthesis in APBs is mediated by BIR, knockdown of POLD3 reduced the telomere synthesis in PML-IV^{GFP}-expressing cells after ABA treatment (Fig. S2C). Using rolling-cycle amplification (RCA) and quantitative PCR (Zhang et al., 2019), we measured the levels of C-circle, a byproduct of ALT. C-circle levels were significantly increased by PML-IV^{GFP} but not PML-IV-3MAS^{GFP} after ABA treatment (Fig. 1G, S2D), confirming that the PML-IV-driven and SUMO-SIM-mediated APB induction stimulates ALT activity. Notably, ABA did not induce telomere synthesis in ALT⁻ U251 MG cells (Fig. S2E). Thus, induction of APBs in ALT$^+$ cells stimulates ALT activity, whereas APB induction in ALT⁻ cells only causes telomere clustering but not ALT activation.

Enhanced ALT telomere synthesis generates replication stress

While using PML-IV-expressing cells to study the effects of APBs on ALT, we surprisingly found that the overall EdU incorporation of cells was reduced by ABA (Fig. 2A). In addition, ABA also induced an increase of G2 cells (Fig. 2A). In contrast, ABA did not reduce EdU incorporation or increase G2 cells in the cell population expressing PML-IV-3MAS^{GFP} (Fig. 2A). Furthermore, PML-V^{GFP}, which failed to induce telomere synthesis when tethered to telomeres (Fig. S3A), did not affect EdU incorporation and the G2 population (Fig. 2A). These results suggest that the induction of telomere synthesis by PML-IV may trigger the ATR checkpoint to inhibit overall DNA synthesis and the G2/M transition. Indeed, ABA increased the phosphorylation of Chk1 (p-Chk1 S345) and RPA32 (p-RPA32 S33), two ATR substrates, in cells expressing PML-IV^{GFP} but not PML-IV-3MAS^{GFP} or PML-V^{GFP} (Fig. 2B). Additionally, ABA induced p-Chk1 and p-RPA32 more robustly in cells expressing high levels of PML-IV^{GFP} than in those expressing PML-IV^{GFP} at low levels (Fig. 2B). The ABA-induced p-Chk1 was dependent on ATR but not ATM (Fig. S3B). Importantly, an induction of RPA32 and p-RPA32 by ABA was observed at telomeres in cells expressing PML-IV^{GFP} (Fig. 2C, S3C), showing that replication stress is generated at telomeres. In contrast, ABA did not induce p-RPA32 at telomeres efficiently in cells expressing PML-IV-3MAS^{GFP} or PML-V^{GFP} (Fig. 2C). These results suggest that PML-IV-induced telomere synthesis generates replication stress and triggers an ATR response.

RAD52 plays an important role in ALT by promoting formation of telomeric D-loops (Zhang et al., 2019). When overexpressed from a doxycycline (DOX)-inducible promoter, RAD52 increased telomere DNA synthesis and telomere FISH intensity (Fig. 2D, lanes 1–2; S3D, lanes 1–2), providing an alternative means to enhance ALT. RAD52 overexpression increased the RPA32 and p-RPA32 at telomeres, as well as p-RPA32 levels (Fig. 2E, lanes 1–2; 2F, lanes 1–2, S3E), supporting the idea that enhanced telomere synthesis generates replication stress. Knockdown of BLM abolished telomere synthesis in the absence and presence of RAD52 overexpression (Fig. 2D, lanes 3–4), and suppressed the RAD52-induced increase of telomere intensity (Fig. S3D, lanes 3–4), confirming that BLM is essential for ALT. The increases of RPA32 at telomeres and p-RPA32 levels in RAD52-overexpressing cells were also eliminated by BLM depletion (Fig. 2E, lanes 3–4; 2F, lanes 3–4), showing that BLM is required for the generation of replication stress. Expression of wild-type BLM (BLM^{WT}) but not the BLM helicase mutants (BLM^{G891E} and BLM^{G901Y}) in cells depleted of endogenous BLM restored telomere synthesis (Fig. 2D, lanes 5–10), the RAD52-induced increase of telomere intensity (Fig. S3D, lanes 5–10), and the induction of RPA32 at telomeres and overall p-RPA32 levels by RAD52 overexpression (Fig. 2E, lanes 5–10; 2F, lanes 5–10), suggesting that the helicase activity of BLM is essential for telomere synthesis and its associated replication stress (Rong et al., 2000). Overexpression of BLM also induced p-RPA32 in G2 cells in a manner dependent on its helicase activity (Fig. S3F). Thus, BLM- and RAD52-driven telomere synthesis is an unexpected source of replication stress at ALT telomeres.

FANCJ and POLD3 contribute to ALT-induced replication stress

The critical function of BLM in ALT prompted us to test whether FANCJ, a helicase associating with BLM (Suhasini et al., 2011), is involved in ALT. Notably, FANCJ was detected at ALT telomeres by previous proteomic studies (Dejardin and Kingston, 2009; Garcia-Exposito et al., 2016). We generated two FANCJ KO U2OS cell lines using CRISPR/Cas9 and tested them for ALT telomere synthesis in APBs (ATSA) (Zhang et al., 2019). Loss of FANCJ did not decrease the number of APBs, but reduced the DNA synthesis at telomeres (Fig. 3A–B, S4A–C). Knockdown of FANCJ with three different siRNAs did not reduce BLM levels but decreased telomere synthesis even in cells overexpressing RAD52 (Fig. 3C, S4D–E). In addition, FANCJ knockdown in cells overexpressing RAD52 reduced the RPA32 at telomeres (Fig. 3D, S4F), indicating a decrease of replication stress. Together, these results suggest that FANCJ promotes ALT telomere synthesis and the associated replication stress.

Given that BLM and RAD52 function in not only BIR but also other DNA repair pathways, we sought to specifically test whether BIR contributes to the replication stress at ALT telomeres. Depletion of POLD3 reduced the induction of p-RPA32 by RAD52 overexpression in G2 cells (Fig. 3E). Knockdown of POLD3 with two independent siRNAs also reduced the RPA32 and p-RPA32 at telomeres in cells overexpressing RAD52 (Fig. 3F). Consistently, in cells expressing PML-IV^{GFP} and $TRF1^{RFP}$, knockdown of POLD3 reduced the ABA-induced increase of p-Chk1 and p-RPA32 (Fig. 3G), as well as the ABA-induced RPA accumulation at telomeres (Fig. S4G). These results demonstrate that BIR is a sources of replication stress at telomeres undergoing robust ALT synthesis.

To test whether the ATR response triggered by BIR is involved in ALT, cells expressing PML-IV^{GFP} and TRF1^{RFP} were simultaneously treated with ABA and the ATR inhibitor (ATRi) VE-821. ATRi reduced telomere synthesis (Fig. 3H). Furthermore, ATRi increased the number of telomere foci but reduced the FISH intensity of telomeres (Fig. 3I), indicating a reduction in telomere clustering. These results are consistent with the function of ATR in promoting ALT (Flynn et al., 2015; Min et al., 2017), and they suggest that the BIR-induced replication stress plays a positive role in ALT.

BLM promotes ALT in APBs by processing BIR intermediates

While BLM is clearly critical for ALT, its specific function in telomeric BIR has been difficult to study because depletion of BLM abolishes APBs, leading to loss of all ALT-associated events. To investigate how BLM functions in APBs, we asked whether tethering of PML-IV to telomeres can bypass the requirement of BLM for APB formation. In cells expressing PML-IV^{GFP} and TRF1^{RFP}, depletion of BLM did not affect the induction of APBs by ABA (Fig. 4A). Furthermore, ABA still reduced the number of telomere foci in BLM knockdown cells (Fig. 4B), indicating telomere clustering. However, ABA did not increase telomere FISH intensity in BLM knockdown cells (Fig. 4C), indicating the lack of telomere synthesis. Indeed, knockdown of BLM abolished the EdU incorporation at telomeres after ABA treatment (Fig. S5A), showing that BLM is essential for telomeric BIR in APBs. Expression of BLM^{WT} but not BLM^{G891E} in BLM knockdown cells restored telomere synthesis (Fig. S5A–B), suggesting that BLM promotes BIR as a helicase in APBs. Furthermore, BLM^{WT} but not BLM^{G891E} restored the increase of p-Chk1 and p-RPA32 (Fig. S5C), as well as the accumulation of RPA32 at telomeres (Fig. S5D), confirming that the helicase activity of BLM is needed for generating replication stress at ALT telomeres.

Unexpectedly, when BLM was depleted from cells induced to form APBs, we observed a drastic increase of anaphase bridges in mitotic cells (Fig. 4D–E). These bridges were positive for both telomere FISH and TRF1 (Fig. 4D), suggesting that certain inter-telomere recombination intermediates are not resolved in the absence of BLM. Depletion of TOP3 and RMI1 also induced telomere bridges in cells with induced APBs (Fig. 4E), suggesting that the BTR complex is required for resolving the intermediates. Notably, expression of BLM^{WT} but not BLM^{G891E} in BLM knockdown cells suppressed the formation of telomere bridges (Fig. 4E), showing that BLM acts as a helicase to resolve the intermediates. Thus, BLM promotes ALT telomere synthesis in APBs by resolving BIR intermediates with its helicase activity.

To characterize the telomere bridges in more detail, we analyzed metaphase spreads of BLM knockdown cells induced to form APBs (Fig. 4F). Bridges between telomeres of different chromosomes and sister chromatids were clearly visible (Fig. 4F). Notably, complex telomere bridges involving >2 chromosomal ends were frequently observed (Fig. 4F), providing evidence for multiple strand invasion events in telomere clusters. The levels of telomere bridges were significantly increased by APB induction (Fig. 4G), suggesting that the BIR intermediates are formed in telomere clusters in APBs.

Next, we asked how the BIR intermediates are generated. Knockdown of MMS21 did not prevent PML-IV-mediated APB formation or reduce the G2/M population of BLM

knockdown cells, but decreased telomere bridges (Fig. 4H, S5E–F), suggesting that MMS21-mediated protein SUMOylation is needed in APBs to generate the intermediates. The strand invasion during BIR requires single-stranded DNA (ssDNA) at collapsed replication forks (Anand et al., 2013). Knockdown of MRE11 and CtIP, two factors involved in DNA end resection, suppressed telomere bridges without reducing the G2/M population (Fig. 4H, S5E). To test whether the functional BIR complex is required to form the intermediates, we knocked down POLD3 with siRNAs (Fig. S5G). Loss of POLD3 reduced telomere bridges (Fig. 4I, S5H), suggesting that the intermediates are formed by the functional BIR complex after strand invasion, possibly in migrating replication bubbles (Kramara et al., 2018).

BLM mediates RAD52-driven BIR and facilitates RAD52 accumulation in APBs

RAD52 promotes telomeric BIR by stimulating D-loop formation in telomeric DNA, and BLM is essential for both RAD52-dependent and -independent BIR pathways (Zhang et al., 2019). Unexpectedly, overexpression of RAD52 reduced the number of telomere foci (Fig. 5A), raising the possibility that BIR itself promotes APB formation and telomere clustering. To test this, we knocked down endogenous BLM in RAD52-overexpressing cells and expressed BLM^{WT}, BLM^{G891E}, or BLM^{C901Y}. Depletion of BLM abolished the reduction in telomere foci caused by RAD52 overexpression, and expression of BLM^{WT} but not BLM^{G891E} and BLM^{C901Y} restored the effect of RAD52 (Fig. 5A). Furthermore, knockdown of BLM in RAD52-overexpressing cells abolished APB formation, which was restored by BLM^{WT} but not BLM^{G891E} and BLM^{C901Y} (Fig. 5B). These results suggest that the helicase activity of BLM is required for RAD52-driven APB formation and telomere clustering.

The role of BLM in RAD52-driven APB formation and telomere clustering is consistent with the function of BLM in resolving BIR intermediates downstream of RAD52. Surprisingly, however, even in cells overexpressing RAD52, the accumulation of RAD52 at telomeres was drastically reduced by BLM knockdown (Fig. 5C). Even in cells expressing PML-IV^{GFP} and $TRF1^{RFP}$, the ABA-induced RAD52 accumulation at telomere was severely compromised by loss of BLM (Fig. 5D). Because PML-IV-induced APB formation is independent of BLM, this result suggests that BLM acts in APBs to promote RAD52 recruitment. Expression of BLM^{WT} but not BLM^{G891E} restored the ABA-induced RAD52 accumulation at telomeres (Fig, 5D), suggesting that the helicase activity of BLM is required for recruiting RAD52 to APBs. Thus, while BLM may function downstream of RAD52 in BIR, it also promotes RAD52 accumulation in APBs, suggesting the presence of a BLM-mediated feedforward loop that enhances RAD52 recruitment.

A BIR-driven feedforward loop to recruit DDR proteins to APBs

Next, we tested whether this BLM-mediated feedforward loop also regulates other DDR proteins in APBs. Overexpression of RAD52 increased the localization of BLM to telomeres (Fig. 6A, S6A). Even in cells overexpressing RAD52, only BLM^{WT} but not BLM^{G891E} and BLM^{C901Y} localized to telomeres efficiently in the absence of endogenous BLM (Fig. 6A–B), suggesting that BLM relies on its own helicase activity to efficiently accumulate in APBs. RAD52 overexpression also increased the telomere localization of other DDR

proteins involved in BIR, such as MRE11 and PCNA (Fig. 6C–D, S6B). Similar to BLM, the efficient localization of MRE11 and PCNA to telomeres was dependent on BLM helicase activity (Fig. 6C–D). Thus, in addition to RAD52 and BLM itself, BLM also promotes the recruitment of other DDR proteins to APBs.

To confirm that the effects of BLM on the recruitment of DDR proteins to APBs are attributed to its function in BIR, we tested whether POLD3 plays a similar role. Even in cells overexpressing RAD52, knockdown of POLD3 reduced the accumulation of both RAD52 and BLM at telomeres (Fig. 6E–F). The accumulation of MRE11 and PCNA at telomeres was also reduced by POLD3 depletion (Fig. S6C–D). Furthermore, in cells induced to form PML-IV-mediated APBs, POLD3 knockdown reduced the accumulation of RAD52 at telomeres (Fig. 6G). These results suggest that BLM and POLD3 function together to promote a BIR-induced feedforward loop that enhances the accumulation of DDR proteins in APBs.

BIR promotes TRF2 SUMOylation

Since telomeric BIR induces replication stress and promotes recruitment of DDR proteins, we asked whether it affects TRF2 SUMOylation, which is critical for ALT telomere synthesis (Min et al., 2019). We pulled down the His-tagged wild-type SUMO2 ($SUMO2^{WT}$) in U2OS cells under a denaturing condition and tested whether TRF2 was covalently modified by SUMO2. A ladder of TRF2 bands were detected in SUMO2 pulldowns (Fig. 7A). The specificity of the TRF2 bands was confirmed by TRF2 knockdown (Fig. S7A), and these bands were increased by RAD52 overexpression and a G2 arrest with CDK1 inhibitor (CDK1i), which increases APB-positive cells (Fig. 7A). In contrast, TRF2 was not detected in the pulldowns of the non-conjugatable SUMO2 mutant ($SUMO2^{NC}$) (Fig. 7A). These results suggest that TRF2 SUMOylation may be stimulated by ALT activity.

To test whether TRF2 SUMOylation is induced by ALT activity, we knocked down PML and BLM. SUMO2-TRF2 was reduced by depletion of PML or BLM, both of which were also SUMOylated (Fig. S7B–C). Notably, expression of BLM^{WT} but not BLM^{G891E} and BLM^{C901Y} restored SUMO2-TRF2 levels in cells depleted of endogenous BLM (Fig. 7B), showing that BLM helicase activity is required for inducing TRF2 SUMOylation. Knockdown of POLD3 also reduced TRF2 SUMOylation (Fig. 7C), confirming that it is driven by BIR. Thus, while TRF2 SUMOylation is required for ALT telomere synthesis, this modification itself is enhanced by telomeric BIR, suggesting that TRF2 SUMOylation is a part of the BIR-driven feedforward loop that perpetuates ALT.

PIAS4 promotes TRF2 SUMOylation and ALT telomere synthesis

MMS21 is known to contribute to TRF2 SUMOylation (Fig. 7D) (Potts and Yu, 2007). Surprisingly, however, depletion of PIAS4, another SUMO ligase detected at ALT telomeres (Garcia-Exposito et al., 2016), reduced SUMO2-TRF2 even more than MMS21 knockdown (Fig. 7D). Overexpression of PIAS4 but not MMS21 increased SUMO2-TRF2 (Fig. S7D). Furthermore, PIAS4 knockdown largely abolished the induction of TRF2 SUMOylation by

RAD52 overexpression (Fig. 7E). These results suggest that PIAS4 mediates the BIR-induced TRF2 SUMOylation.

If the BIR-driven feedforward loop is mediated by PIAS4, PIAS4 should be important for the recruitment of DDR proteins to APBs and telomere synthesis. Indeed, even in cells overexpressing RAD52, knockdown of PIAS4 reduced the accumulation of RAD52 at telomeres (Fig. 7F, S7E). In addition, PIAS4 depletion decreased the RPA32 at telomeres (Fig. S7F–G), as well as p-RPA32 levels (Fig. S7H), indicating a reduction in replication stress. Knockdown of PIAS4 reduced telomere synthesis, which was rescued by siRNA-resistant wild-type PIAS4 (Fig. 7G, S7I). The DNA synthesis at telomeres was also reduced in two independent PIAS4 KO cell lines when RAD52 was overexpressed (Fig. 7H). Furthermore, overexpression of PIAS4 reduced the number of telomere foci, increased telomere intensity, and enhanced telomere synthesis (Fig. S7J–K). These results demonstrate the contribution of PIAS4 to ALT telomere synthesis, suggesting that PIAS4 is a key mediator of the BIR-driven feedforward loop perpetuating ALT.

Discussion

Recent studies suggested that ALT is triggered by DNA damage or replication stress at telomeres, and is mediated by BIR (Dilley et al., 2016; O'Sullivan et al., 2014; Roumelioti et al., 2016; Sobinoff et al., 2017; Zhang et al., 2019). Furthermore, ALT occurs in APBs in G2 and M phases, and APBs are critical for efficient ALT telomere synthesis (Loe et al., 2020; Min et al., 2017, 2019; Ozer et al., 2018; Zhang et al., 2019). Although the framework of the ALT pathway has gradually emerged, several important questions about this pathway remained unanswered. For example, it is still unclear why telomeric replication stress preferentially activates ALT in ALT^+ cells. It is also unclear how ALT occurs in APBs. Moreover, while it is evident that BLM is a key regulator of ALT (Min et al., 2019; Sobinoff et al., 2017; Zhang et al., 2019), how BLM functions in telomeric BIR remains largely unknown. The findings of this study reveal that telomeric BIR is an unexpected source of replication stress, and this stress drives a SUMOylation-mediated feedforward loop to recruit DDR proteins to APBs and perpetuate ALT activity (Fig. 7I). Using PML-IV to directly promote APB formation, we recreated a unique state of ALT telomeres that allows us to interrogate the function of BLM in BIR. Our data show that BLM promotes BIR by processing inter-telomere BIR intermediates, unveiling a key function of BLM in ALT. Collectively, these findings suggest that ALT is a self-perpetuating process driven by a BIR-triggered feedforward loop in APBs, offering explanations of how ALT is stably activated by telomeric replication stress in ALT^+ cells, why ALT occurs in APBs, and how BLM functions in APBs to drive ALT.

A previous study showed that tethering of PML-III to *lacO* repeats at subtelomeric loci induced *de novo* APB formation and telomere synthesis (Chung et al., 2011). Consistent with this study, we found that tethering of PML-IV to telomeric repeats also induced APB and telomere synthesis robustly. However, there are several noticeable differences between the two studies. First, we found that PML-IV is the main PML variant that functionally supports ALT. Second, by targeting PML-IV to endogenous telomeric repeats, we avoid the potential contribution of *lacO* repeats to replication stress. Third, only the tethering of PML-

IV to endogenous telomeric repeats promotes telomere clustering, recapitulating a key feature of ALT telomeres. Finally, we show that although tethering of PML-IV to telomeres is sufficient to induce APBs and telomere clustering in both ALT^+ and ALT^- cells, it only enhances telomere synthesis in ALT^+ cells, suggesting that APB formation is a mechanism to enhance but not to initiate ALT. The unique ability of PML-IV to support APB formation may stem from its interaction with endogenous TRF1 and other proteins in APBs (Yu et al., 2010). Two recent studies showed that tethering a poly(SUMO)-poly(SIM) fusion protein or SIM to telomeres induces APB formation through SUMO-SIM-mediated phase separation (Min et al., 2019; Zhang et al., 2020). Consistent with these studies, we also found that SUMO-SIM-mediated interactions are critical for the formation of PML-IV-induced APBs. Together, these studies strongly suggest that APB formation is a process driven by phase separation, which brings telomeres together and allows ALT to occur between chromosomes (Fig. 7I). Notably, however, tethering of PML-IV but not SIM to telomeres in ALT^+ U2OS cells enhanced the accumulation of DDR proteins in APBs (Zhang et al., 2020), suggesting that PML-IV plays an important role in organizing protein-protein interactions in APBs. Thus, the inducible tethering of PML-IV to telomeres provides a unique approach to study how functional APBs are formed and how ALT occurs in APBs.

In addition to clustering telomeres, APBs also bring in DDR proteins to promote ALT. A recent study showed that tethering of RMI1 to telomeres restored ALT in PML KO cells, suggesting that the key function of APB is to recruit BLM (Loe et al., 2020). Nonetheless, how BLM functions in APBs remains unclear. The direct induction of APBs by tethering PML-IV to telomeres provides us with an opportunity to bypass the requirement of BLM for APB formation, allowing us to examine how BLM works in APBs. Using this approach, we found that BLM is essential for telomere synthesis in APBs. Furthermore, ablation of BLM helicase activity in APBs led to accumulation of inter-telomere bridges in mitotic cells, providing direct evidence showing that BLM is required for processing inter-telomere BIR intermediates.

A key event during BIR is the migration of replication bubbles (Kramara et al., 2018). During bubble migration, two helicase activities may be needed to unwind double-stranded template DNA and separate the nascent leading strand from its template (Kramara et al., 2018). It is possible that BLM drives bubble migration by promoting these unwinding events. In the absence of BLM, BIR is stuck after strand invasion, explaining how inter-telomere bridges are formed. Indeed, the BIR intermediates that accumulate in the absence of BLM are formed in a POLD3-dependent manner, suggesting that these intermediates are formed in BIR bubbles and may require BIR-mediated DNA synthesis. Interestingly, FANCJ, a helicase that associates with BLM but has the opposite directionality (Cantor et al., 2004; Karow et al., 1997), also contributes to ALT activity. The possibility that BLM and FANCJ function together to promote migration of replication bubbles during BIR warrants careful biochemical studies.

Another surprising finding of this study is that BIR is a source of replication stress. BIR is commonly viewed as a repair mechanism that rescues collapsed replication forks (Anand et al., 2013). However, BIR itself is a type of aberrant DNA replication. During BIR, the nascent leading strand serves as the template for lagging strand synthesis, creating DNA

intermediates not present at normal replication forks (Kramara et al., 2018). Consistent with our findings, BIR increases telomere fragility in ALT$^+$ cells (Yang et al., 2020). The finding that telomeric BIR is a source of replication stress suggests that ALT is not simply passively induced by telomeric replication problems, but it also fuels the stress at telomeres. This finding also indicates that ALT is a self-perpetuating process, explaining how ALT is stably activated in ALT$^+$ cells once it is triggered by replication stress.

This study also uncovers an unexpected feedforward loop triggered by BIR and mediated by PIAS4, explaining how ALT perpetuates itself. While MMS21 is important for ALT, PIAS4 may be the primary SUMO ligase that promotes TRF2 SUMOylation and drives the feedforward loop in APBs (Fig. 7I). The enhanced SUMOylation of TRF2 and other proteins in APBs helps recruit DDR proteins, leading to growth of APBs and increased enrichment of DDR proteins at telomeres (Fig. 7I). This enrichment of DDR proteins in APBs may enhance ongoing BIR and initiate new BIR events in telomere clusters, perpetuating ALT activity.

In a big picture, ALT is triggered by DNA replication stress and becomes self-perpetuating in APBs (Fig. 7I). In ALT$^+$ cells, many events that promote the feedforward loop, such as APB induction and BLM overexpression, can stimulate ALT (Min et al., 2019; Sobinoff et al., 2017). However, these events are typically insufficient to activate ALT in ALT$^-$ cells. In some extreme situations, such as combining APB induction and BLM overexpression (Min et al., 2019), or introducing high levels of replication stress or DNA damage to telomeres (Dilley et al., 2016; O'Sullivan et al., 2014), ALT activity could be induced in ALT$^-$ cells. In cancer cells, the telomeric replication stress required to trigger the feedforward loop may define the threshold of replication stress to activate ALT. Furthermore, APBs provide a dynamic environment critical for the feedforward loop to operate, explaining the spatial and temporal regulation of ALT during the cell cycle. It is tempting to speculate that naturally occurring ALT is driven by three critical events: (1) the initial DNA damage response at telomeres, (2) the clustering of telomeres by SUMO-SIM-mediated phase separation, and (3) the BIR-driven feedforward loop in APBs (Fig. 7I). This model may help us understand how ALT is activated in cancer cells, how different DDR and telomere proteins modulate ALT activity, and how to target the ALT pathway effectively in cancer therapy.

Limitations

While FANCJ contributes to ALT activity, the exact role of FANCJ in BIR remains unclear. Further investigations are needed to understand how FANCJ functions with BLM and other BIR proteins. Elucidation of the role of FANCJ in ALT may provide insights into the helicase activities driving BIR, shedding light on how BIR operates at telomeres.

STAR★METHODS

Detailed methods are provided in the online version of this paper and include the following:

RESOURCE AVAILABILITY

Lead Contact—Further information and requests for resources and reagents should be directed to and will be fulfilled by the Lead Contact, Dr. Lee Zou

(zou.lee@mgh.harvard.edu), Massachusetts General Hospital Cancer Center, Harvard medical School, Boston, MA 02129, USA.

Materials Availability—All unique reagents generated in this study will be made available upon request, but we may require a payment and/or a completed Materials Transfer Agreement if there is potential for commercial application.

Data and Code Availability—Western blot and immunofluorescence raw data can be accessed in Mendeley: https://data.mendeley.com/datasets/f4ysyn9t58/3 This study did not generate any unique datasets or code.

EXPERIMENTAL MODEL AND SUBJECT DETAILS

Cell culture—RPE-1, U2OS and its derivative RAD52-inducible (RAD52 OE), PIAS4-inducible (PIAS4 OE), MMS21-inducible (MMS21 OE), FANCJ KO and PIAS4 KO cell lines were cultured in DMEM supplemented with 10% fetal bovine serum (FBS), 2mM Glutamine and 1% penicillin/streptomycin. U-251 MG was cultured in DMEM/F12 supplemented with 10% FBS and 1% penicillin/streptomycin. To generate the RAD52-inducible cell line, U2OS cells were infected with lentiviruses expressing RAD52 from a Dox-inducible promoter (pInducer20-RAD52). To generate the PIAS4-inducible cell line, WT U2OS or RAD52 OE U2OS cells expressing 10xHis-SUMO2^{WT} were infected with lentiviruses expressing siRNA-resistant PIAS4 from a Dox-inducible promoter (pInducer20-PIAS4). To generate the MMS21-inducible cell line, RAD52 OE U2OS cells expressing 10xHis-SUMO2^{WT} were infected with lentiviruses expressing MMS21 from a Dox-inducible promoter (pInducer20-MMS21). FANCJ KO and PIAS4 KO cells were generated with CRISPR/Cas9 as described below.

Cell lines—To conditionally tether PML-IV to telomeres, U2OS cells were infected with lentiviruses expressing TRF1^{RFP} (pLenti PGK PYL1-TagRFP-TRF1) and PML-IV-WT^{GFP} or PML-IV-3MAS^{GFP} (pLenti PGK ABI-EGFP-PMLIV-WT or −3MAS). To generate the RAD52-inducible cell line, U2OS cells were infected with lentiviruses expressing RAD52 from a Dox-inducible promoter (pInducer20-RAD52-HA). To express BLM in U2OS and its derivative cells, cells were infected with lentiviruses expressing siRNA-resistant wild-type BLM or mutants (pHAGE-EF1a-3*HA-BLM-siR-WT, G891E, or -C901Y). To generate the PIAS4-inducible cell line, wild-type or RAD52 OE U2OS cells expressing 10xHis-SUMO2^{WT} were infected with lentiviruses expressing siRNA-resistant PIAS4 from a Dox-inducible promoter (pInducer20-PIAS4-siR-HA). To generate the MMS21-inducible cell line, RAD52 OE U2OS cells expressing 10xHis-SUMO2^{WT} were infected with lentiviruses expressing MMS21 from a Dox-inducible promoter (pInducer20-MMS21-siR-HA). FANCJ KO and PIAS4 KO cells were generated with CRISPR/Cas9 as described below.

METHOD DETAILS

Generation of KO cell lines—The DNA sequences encoding sgRNAs (see blew) were cloned into the PX458 vector. Four days after the sgRNA-expressing plasmids were transfected into U2OS cells, the top 10% GFP^{+} cells were isolated by cell sorting. Loss of

the target proteins was verified by western blot. The whole populations of sorted cells were used in the experiments as shown in figures.

FANCJ KO#1 was generated in U2OS cells using the FANCJ sgRNA combination #01 (TCCGGAGGACGGCATATTCA and GTCATCGAATACCATTAAGA). FANCJ KO#2 was generated in U2OS cells using the FANCJ sgRNA combination #02 (CCGGAGCTCTCTAGTAATCT and GTCATCGAATACCATTAAGA). PIAS4 KO#1 was generated in RAD52-inducible U2OS cells using the PIAS4 sgRNA combination #01 (TACTCCGGCCCACGAAACCC and GTAGGTGGAGTGCATGGTCA). PIAS4 KO#2 was generated in RAD52-inducile U2OS cells using the PIAS4 sgRNA combination #02 (TGAAGCACGAGCTCGTCACC and AGCGCCGGCCCGGTCGTAGG).

RNA interference—siRNA transfections were done by reverse transfection with Lipofectamine RNAiMax (Invitrogen). All siRNAs were transfected at 5–10 nM. For the C-circle assay, cells were collected 96 h post transfection. For cell synchronization in G2, cells were treated with CDK1i (RO-3306, 15 μM) at 72 h after siRNA transfection. For tethering PML-IV to telomeres using ABA, cells were treated with ABA (200 μM) at 72 h after siRNA transfection. A list of the siRNAs used in this study is in supplemental material Table S1.

Cell-cycle analysis (FACS)—U2OS cells expressing $TRF1^{RFP}$ and PML-IV-WT^{GFP}, or indicated PML variants were treated with DMSO or ABA (200 μM) for 18 h, pulsed with EdU (10 μM) for 30 minutes, and then fixed in 75% ethanol at −20°C overnight. The samples were processed with the Click-iT EdU Alexa Fluor 647 Flow Cytometry Assay Kit (Thermo Fisher Scientific C10635) following the manufacturer's recommendations. The cell pellets were resuspended in 10 μg/mL Propidium Iodide (PI) and 50 μg/mL RNaseA at 37°C for 20 minutes. Flow cytometry was done using a BD LSRII apparatus equipped with the FACS Diva software (BD Biosciences).

Detection of DNA synthesis at telomeres—To visualize DNA synthesis in PML-IV-induced APBs, U2OS cells expressing $TRF1^{RFP}$ and PML-IV-WT^{GFP}, or indicated PML variants were treated with DMSO or ABA (200 μM) for 18 h, and then incubated with EdU (20 μM) for 1 h. To visualize DNA synthesis at telomeres in other contexts, U2OS cells were synchronized in G2 with CDK1i (RO-3306, 15 μM) for 18 h, and then incubated with EdU (20 μM) for 1 h. To induce PIAS4 expression, PIAS4-inducible U2OS cells were treated with 50 or 100 ng/ml Dox 6 h before synchronization in G2 with CDK1i.

For immunofluorescence of EdU, cells on coverslips were cooled on ice, rinsed once with 1x PBS, treated with pre-extraction buffer (0.1% Triton X-100, 20 mM HEPES-KOH pH 7.9, 50 mM NaCl, 300 mM sucrose) for 5 min on ice, rinsed once with 1x PBS, fixed with PFA for 18 min at RT, and then permeabilized in PBS with 0.5%Triton X-100 for 5 min. After rinsing cells with PBS containing 3% BSA, EdU was labeled with Biotin through click-iT reaction. Cells were incubated in blocking solution (1xPBS containing 0.05% Tween-20 and 3% BSA) for 1h at RT, and in anti-biotin antibody (ab53494, Abcam, 1:500) diluted in blocking solution for 2 h at RT or overnight at 4°C. After 3x washes with PBST (1xPBS containing 0.05% Tween-20), cells were incubated in secondary antibodies conjugated to

594 fluorophores in the same blocking solution for 1 h at RT. After 3x washes with PBST, cells were fixed again with PFA for 15 min at RT, dehydrated in 70%, 85%, and 100% ethanol for 2 min each, and allowed to air dry completely. Cells on coverslips were incubated with 20 μL preheated hybridizing solution (70% formamide, 2x SSC, 2 mg/ml BSA, 10% dextran sulfate) containing 100 nM TelC-Alexa488 (F1004, PNA Bio), the PNA probe for telomeric DNA, and denatured for 10 min at 85°C on a heat block. After incubation at RT in the dark for 2 h, cells were washed with washing solution (70% formamide, 2x SSC) three times for 5 min each and 2x SSC, 0.1% tween-20 three times for 5 min each. During the second wash, cells were stained with DAPI. The images were captured with a Nikon 90i microscope.

Detection of DDR proteins at telomeres—Immunofluorescence analysis of DDR factors at PML-IV-induced APBs was performed after 14 h ABA (200 μM) treatment. Immunofluorescence analysis of DDR factors at telomeres in other contexts was performed in G2 cells synchronized by 18 h CDK1i (RO3306, 15 μM) treatment. Cells were pre-extracted with pre-extraction buffer (0.1% Triton X-100, 20 mM HEPES-KOH pH 7.9, 50 mM NaCl, 300 mM sucrose), fixed with PFA, permeabilized in PBS with 0.5%Triton X-100, and incubated in blocking solution (1xPBS containing 0.05% Tween-20 and 3% BSA). Subsequently, cells were successively incubated in primary antibodies and secondary antibodies diluted in same blocking solution. Three washes with PBST were done between each step. Telomere FISH was done as described above. Images were captured at 60X or 20X using Nikon 90i microscope.

Detection of telomere bridges—Cells were fixed by PFA for 15 min after an 18-h ABA (200 μM) treatment. After permeabilization in PBS with 0.5%Triton X-100 for 5 mins, cells were stained with DAPI for 5 min and wash once with PBST. Images of $TRF1^{RFP}$ and $PML\text{-}IV^{GFP}$ were directly captured using 20x Nikon 90i or Echo-7 microscope.

For metaphase chromosome spread, U2OS cells expressing $TRF1^{RFP}$ and $PML\text{-}IV^{GFP}$ were transfected with BLM siRNA, and then treated with 200 μM DMSO or ABA for 12 h, and 20 ng/ml colcemid for another 4 h. Mitotic cells were harvested, incubated with 75 mM KCl at 37 °C for 20 min, and prefixed with several drops of ice-cold fixation buffer (methanol:acetic acid, 3:1). Cells were pelleted, resuspended with ice-cold fixation buffer, and fixed for 10 min. After three washes with fixation buffer, cells were dropped on ethanol-water washed slides. After air dry overnight, telomere signals were detected by FISH.

Time-lapse imaging of telomere fusion—U2OS cells expressing $TRF1^{RFP}$ and $PML\text{-}IV^{GFP}$ were cultured in 15-mm glass bottom cell culture dishes. After 10 h of exposure to ABA, the fluorescence of $TRF1^{RFP}$ and $PML\text{-}IV\text{-}WT^{GFP}$ in live cells was directly analyzed with an Olympus FV1000 IX2 inverted confocal microscope at room temperature for 2 h. Images of $TRF1^{RFP}$ and $PML\text{-}IV^{GFP}$ were taken every 2 min.

C-circle assay—C-circle assay was performed as previously described (Lau et al., 2013). Genomic DNA was prepared with PureLink Genomic DNA Mini Kit (K182002). Diluted DNA (16 ng) was incubated with 0.2 mg/ml BSA, 0.1% Tween, 4mM dithiothreitol (DTT), 1 mM each dNTP without dCTP, 1× φ29 Buffer (NEB) and 7.5 U φ29 DNA polymerase

(NEB) at 30 °C for 8 h, and then 65 °C for 20 min. For RCA(+) and RCA(−) samples, the assay was done with or without φ29 DNA polymerase respectively. The levels of telomeric DNA in RCA(−) and RCA(+) samples were determined by qPCR. C-circles are calculated by ΔCt (RCA+)/ΔCt (RCA −). For each control or knockdown condition, triplicated samples were used for the quantification of C-circles. A list of the primers used in the C-circle assay is in supplemental material Table S2.

SUMOylation of TRF2—SUMOylated proteins were enriched as described (Tatham et al., 2009). RAD52-inducible U2OS cells expressing 10xHis-SUMO2^{WT} or the non-conjugatable SUMO2 mutant 10xHis-SUMO2^{NC} (SUMO2-ΔGG) were transfected with siRNA as indicated. For overexpression of RAD52, Dox was added at 24 h after siRNA transfection. To synchronize cells in G2, cells were treated with CDK1i at 72 h after siRNA transfection. After 20 h of CDK1i treatment, approximately 8× 10^6 cells were collected for each sample. After 1x PBS wash, cell pellets were resuspended in 1 ml PBS. A fraction (40 ul) of the cell suspensions was kept as input. The rest of the cell suspensions were centrifuged, and cell pellets were lysed with denaturing buffer (6 M GuHCl, 100 mM sodium phosphate, 10 mM Tis-HCl, 20 mM imidazole, 5mM β-ME, pH=8.0). Ni-NTA beads (40ul for each sample) were washed three times with PBS and once with denaturing buffer, and then incubated together with the lysates at 4°C overnight. Subsequently, Ni-NTA beads were washes once with denaturing buffer, and three times with washing buffer (8M Urea 100 mM sodium phosphate, 10 mM imidazole, 5 mM β-ME, 0.1% Triton X-100, pH=6.3). Finally, the proteins captured by Ni-NTA beads were eluted three times by boiling in 2x loading buffer containing 250 mM imidazole. The levels of TRF2, SUMO2, and other indicated proteins in input and pull-down samples were analyzed by western blot.

QUANTIFICATION AND STATISTICAL ANALYSIS—Statistical parameters are shown in figures and figure legends. For DNA synthesis analysis at telomeres, only non-S phase cells were used for quantification. When the intensity of DDR factors, EdU and telomere FISH were analyzed, the colocalization and intensity of these signals were quantified together using the FociLab 2.0 software developed by Dr. Li-Lin Du's lab. GraphPad Prism 7 was the software used for statistical analysis. As described in figure legends, unpaired Student's t test was used for statistical analysis, and standard deviations (SD) are shown.

Supplementary Material

Refer to Web version on PubMed Central for supplementary material.

Acknowledgements

We thank Drs. R. Everett, J. Shay, and T. Yadav for reagents, and members of Zou, Dyson, Lan and Elia labs for discussions. J.-M.Z. is a recipient of the Massachusetts General Hospital Cancer Center Excellence Award. L.Z. is the James & Patricia Poitras Endowed Chair in Cancer Research. This work is supported by grants from the NIH grants CA197779, CA248526, and CA218856 to L.Z.

References

Amato R, Valenzuela M, Berardinelli F, Salvati E, Maresca C, Leone S, Antoccia A, and Sgura A. (2020). G-quadruplex Stabilization Fuels the ALT Pathway in ALT-positive Osteosarcoma Cells. Genes (Basel) 11.

Anand RP, Lovett ST, and Haber JE (2013). Break-induced DNA replication. Cold Spring Harb Perspect Biol 5, a010397.

Arora R, Lee Y, Wischnewski H, Brun CM, Schwarz T, and Azzalin CM (2014). RNaseH1 regulates TERRA-telomeric DNA hybrids and telomere maintenance in ALT tumour cells. Nat Commun 5, 5220. [PubMed: 25330849]

Banani SF, Rice AM, Peeples WB, Lin Y, Jain S, Parker R, and Rosen MK (2016). Compositional Control of Phase-Separated Cellular Bodies. Cell 166, 651–663. [PubMed: 27374333]

Barroso-Gonzalez J, Garcia-Exposito L, Hoang SM, Lynskey ML, Roncaioli JL, Ghosh A, Wallace CT, Modesti M, Bernstein KA, Sarkar SN, et al. (2019). RAD51AP1 Is an Essential Mediator of Alternative Lengthening of Telomeres. Mol Cell 76, 11–26 e17. [PubMed: 31400850]

Cantor S, Drapkin R, Zhang F, Lin Y, Han J, Pamidi S, and Livingston DM (2004). The BRCA1-associated protein BACH1 is a DNA helicase targeted by clinically relevant inactivating mutations. Proc Natl Acad Sci U S A 101, 2357–2362. [PubMed: 14983014]

Cesare AJ, Kaul Z, Cohen SB, Napier CE, Pickett HA, Neumann AA, and Reddel RR (2009). Spontaneous occurrence of telomeric DNA damage response in the absence of chromosome fusions. Nat Struct Mol Biol 16, 1244–1251. [PubMed: 19935685]

Chen Q, Ijpma A, and Greider CW (2001). Two survivor pathways that allow growth in the absence of telomerase are generated by distinct telomere recombination events. Mol Cell Biol 21, 1819–1827. [PubMed: 11238918]

Chung I, Leonhardt H, and Rippe K. (2011). De novo assembly of a PML nuclear subcompartment occurs through multiple pathways and induces telomere elongation. J Cell Sci 124, 3603–3618. [PubMed: 22045732]

Dejardin J, and Kingston RE (2009). Purification of proteins associated with specific genomic Loci. Cell 136, 175–186. [PubMed: 19135898]

Dilley RL, and Greenberg RA (2015). ALTernative Telomere Maintenance and Cancer. Trends Cancer 1, 145–156. [PubMed: 26645051]

Dilley RL, Verma P, Cho NW, Winters HD, Wondisford AR, and Greenberg RA (2016). Break-induced telomere synthesis underlies alternative telomere maintenance. Nature 539, 54–58. [PubMed: 27760120]

Draskovic I, Arnoult N, Steiner V, Bacchetti S, Lomonte P, and Londono-Vallejo A. (2009). Probing PML body function in ALT cells reveals spatiotemporal requirements for telomere recombination. Proc Natl Acad Sci U S A 106, 15726–15731. [PubMed: 19717459]

Flynn RL, Cox KE, Jeitany M, Wakimoto H, Bryll AR, Ganem NJ, Bersani F, Pineda JR, Suva ML, Benes CH, et al. (2015). Alternative lengthening of telomeres renders cancer cells hypersensitive to ATR inhibitors. Science 347, 273–277. [PubMed: 25593184]

Garcia-Exposito L, Bournique E, Bergoglio V, Bose A, Barroso-Gonzalez J, Zhang S, Roncaioli JL, Lee M, Wallace CT, Watkins SC, et al. (2016). Proteomic Profiling Reveals a Specific Role for Translesion DNA Polymerase eta in the Alternative Lengthening of Telomeres. Cell Rep 17, 1858–1871. [PubMed: 27829156]

Grobelny JV, Godwin AK, and Broccoli D. (2000). ALT-associated PML bodies are present in viable cells and are enriched in cells in the G(2)/M phase of the cell cycle. J Cell Sci 113 Pt 24, 4577–4585. [PubMed: 11082050]

Heaphy CM, Subhawong AP, Hong SM, Goggins MG, Montgomery EA, Gabrielson E, Netto GJ, Epstein JI, Lotan TL, Westra WH, et al. (2011). Prevalence of the alternative lengthening of telomeres telomere maintenance mechanism in human cancer subtypes. Am J Pathol 179, 1608–1615. [PubMed: 21888887]

Henson JD, and Reddel RR (2010). Assaying and investigating Alternative Lengthening of Telomeres activity in human cells and cancers. FEBS Lett 584, 3800–3811. [PubMed: 20542034]

Hoang SM, and O'Sullivan RJ (2020). Alternative Lengthening of Telomeres: Building Bridges To Connect Chromosome Ends. Trends Cancer 6, 247–260. [PubMed: 32101727]

Jacome A, and Fernandez-Capetillo O. (2011). Lac operator repeats generate a traceable fragile site in mammalian cells. EMBO Rep 12, 1032–1038. [PubMed: 21836640]

Jensen K, Shiels C, and Freemont PS (2001). PML protein isoforms and the RBCC/TRIM motif. Oncogene 20, 7223–7233. [PubMed: 11704850]

Karow JK, Chakraverty RK, and Hickson ID (1997). The Bloom's syndrome gene product is a 3'−5' DNA helicase. J Biol Chem 272, 30611–30614. [PubMed: 9388193]

Kramara J, Osia B, and Malkova A. (2018). Break-Induced Replication: The Where, The Why, and The How. Trends Genet 34, 518–531. [PubMed: 29735283]

Lau LM, Dagg RA, Henson JD, Au AY, Royds JA, and Reddel RR (2013). Detection of alternative lengthening of telomeres by telomere quantitative PCR. Nucleic Acids Res 41, e34.

Liang FS, Ho WQ, and Crabtree GR (2011). Engineering the ABA plant stress pathway for regulation of induced proximity. Sci Signal 4, rs2.

Loe TK, Li JSZ, Zhang Y, Azeroglu B, Boddy MN, and Denchi EL (2020). Telomere length heterogeneity in ALT cells is maintained by PML-dependent localization of the BTR complex to telomeres. Genes Dev 34, 650–662. [PubMed: 32217664]

Lu R, O'Rourke JJ, Sobinoff AP, Allen JAM, Nelson CB, Tomlinson CG, Lee M, Reddel RR, Deans AJ, and Pickett HA (2019). The FANCM-BLM-TOP3A-RMI complex suppresses alternative lengthening of telomeres (ALT). Nat Commun 10, 2252. [PubMed: 31138797]

Min J, and Shay JW (2019). Telomere clustering drives ALT. Aging (Albany NY) 11, 8046–8047. [PubMed: 31612868]

Min J, Wright WE, and Shay JW (2017). Alternative Lengthening of Telomeres Mediated by Mitotic DNA Synthesis Engages Break-Induced Replication Processes. Mol Cell Biol 37.

Min J, Wright WE, and Shay JW (2019). Clustered telomeres in phase-separated nuclear condensates engage mitotic DNA synthesis through BLM and RAD52. Genes Dev 33, 814–827. [PubMed: 31171703]

Neumann AA, Watson CM, Noble JR, Pickett HA, Tam PP, and Reddel RR (2013). Alternative lengthening of telomeres in normal mammalian somatic cells. Genes Dev 27, 18–23. [PubMed: 23307865]

O'Sullivan RJ, Arnoult N, Lackner DH, Oganesian L, Haggblom C, Corpet A, Almouzni G, and Karlseder J. (2014). Rapid induction of alternative lengthening of telomeres by depletion of the histone chaperone ASF1. Nat Struct Mol Biol 21, 167–174. [PubMed: 24413054]

Ozer O, Bhowmick R, Liu Y, and Hickson ID (2018). Human cancer cells utilize mitotic DNA synthesis to resist replication stress at telomeres regardless of their telomere maintenance mechanism. Oncotarget 9, 15836–15846. [PubMed: 29662610]

Pan X, Drosopoulos WC, Sethi L, Madireddy A, Schildkraut CL, and Zhang D. (2017). FANCM, BRCA1, and BLM cooperatively resolve the replication stress at the ALT telomeres. Proc Natl Acad Sci U S A 114, E5940–E5949. [PubMed: 28673972]

Potts PR, and Yu H. (2007). The SMC5/6 complex maintains telomere length in ALT cancer cells through SUMOylation of telomere-binding proteins. Nat Struct Mol Biol 14, 581–590. [PubMed: 17589526]

Rong SB, Valiaho J, and Vihinen M. (2000). Structural basis of Bloom syndrome (BS) causing mutations in the BLM helicase domain. Mol Med 6, 155–164. [PubMed: 10965492]

Roumelioti FM, Sotiriou SK, Katsini V, Chiourea M, Halazonetis TD, and Gagos S. (2016). Alternative lengthening of human telomeres is a conservative DNA replication process with features of break-induced replication. EMBO Rep 17, 1731–1737. [PubMed: 27760777]

Shay JW, Reddel RR, and Wright WE (2012). Cancer. Cancer and telomeres--an ALTernative to telomerase. Science 336, 1388–1390. [PubMed: 22700908]

Shay JW, and Wright WE (2019). Telomeres and telomerase: three decades of progress. Nat Rev Genet 20, 299–309. [PubMed: 30760854]

Shen TH, Lin HK, Scaglioni PP, Yung TM, and Pandolfi PP (2006). The mechanisms of PML-nuclear body formation. Mol Cell 24, 331–339. [PubMed: 17081985]

Silva B, Pentz R, Figueira AM, Arora R, Lee YW, Hodson C, Wischnewski H, Deans AJ, and Azzalin CM (2019). FANCM limits ALT activity by restricting telomeric replication stress induced by deregulated BLM and R-loops. Nat Commun 10, 2253. [PubMed: 31138795]

Sobinoff AP, Allen JA, Neumann AA, Yang SF, Walsh ME, Henson JD, Reddel RR, and Pickett HA (2017). BLM and SLX4 play opposing roles in recombination-dependent replication at human telomeres. EMBO J 36, 2907–2919. [PubMed: 28877996]

Sobinoff AP, and Pickett HA (2020). Mechanisms that drive telomere maintenance and recombination in human cancers. Curr Opin Genet Dev 60, 25–30. [PubMed: 32119936]

Suhasini AN, Rawtani NA, Wu Y, Sommers JA, Sharma S, Mosedale G, North PS, Cantor SB, Hickson ID, and Brosh RM Jr. (2011). Interaction between the helicases genetically linked to Fanconi anemia group J and Bloom's syndrome. EMBO J 30, 692–705. [PubMed: 21240188]

Tatham MH, Rodriguez MS, Xirodimas DP, and Hay RT (2009). Detection of protein SUMOylation in vivo. Nat Protoc 4, 1363–1371. [PubMed: 19730420]

Verma P, Dilley RL, Zhang T, Gyparaki MT, Li Y, and Greenberg RA (2019). RAD52 and SLX4 act nonepistatically to ensure telomere stability during alternative telomere lengthening. Genes Dev 33, 221–235. [PubMed: 30692206]

Yang Z, Takai KK, Lovejoy CA, and de Lange T. (2020). Break-induced replication promotes fragile telomere formation. Genes Dev 34, 1392–1405. [PubMed: 32883681]

Yeager TR, Neumann AA, Englezou A, Huschtscha LI, Noble JR, and Reddel RR (1999). Telomerase-negative immortalized human cells contain a novel type of promyelocytic leukemia (PML) body. Cancer Res 59, 4175–4179. [PubMed: 10485449]

Yu J, Lan J, Wang C, Wu Q, Zhu Y, Lai X, Sun J, Jin C, and Huang H. (2010). PML3 interacts with TRF1 and is essential for ALT-associated PML bodies assembly in U2OS cells. Cancer Lett 291, 177–186. [PubMed: 19900757]

Zhang H, Zhao R, Tones J, Liu M, Dilley R, Chenoweth DM, Greenberg RA, and Lampson MA (2020). Nuclear body phase separation drives telomere clustering in ALT cancer cells. Mol Biol Cell, mbcE19100589.

Zhang J, Dewar JM, Budzowska M, Motnenko A, Cohn MA, and Walter JC (2015). DNA interstrand cross-link repair requires replication-fork convergence. Nat Struct Mol Biol 22, 242–247. [PubMed: 25643322]

Zhang JM, Yadav T, Ouyang J, Lan L, and Zou L. (2019). Alternative Lengthening of Telomeres through Two Distinct Break-Induced Replication Pathways. Cell Rep 26, 955–968 e953. [PubMed: 30673617]

Zhang JM, and Zou L. (2020). Alternative lengthening of telomeres: from molecular mechanisms to therapeutic outlooks. Cell Biosci 10, 30. [PubMed: 32175073]

Highlights

1. Tethering of PML-IV to telomeres induces *de novo* APBs and stimulates ALT.
2. ALT generates replication stress in APBs through BIR.
3. BLM promotes ALT by resolving BIR intermediates in APBs.
4. A BIR-driven and SUMO-mediated feedforward loop perpetuates ALT in APBs.

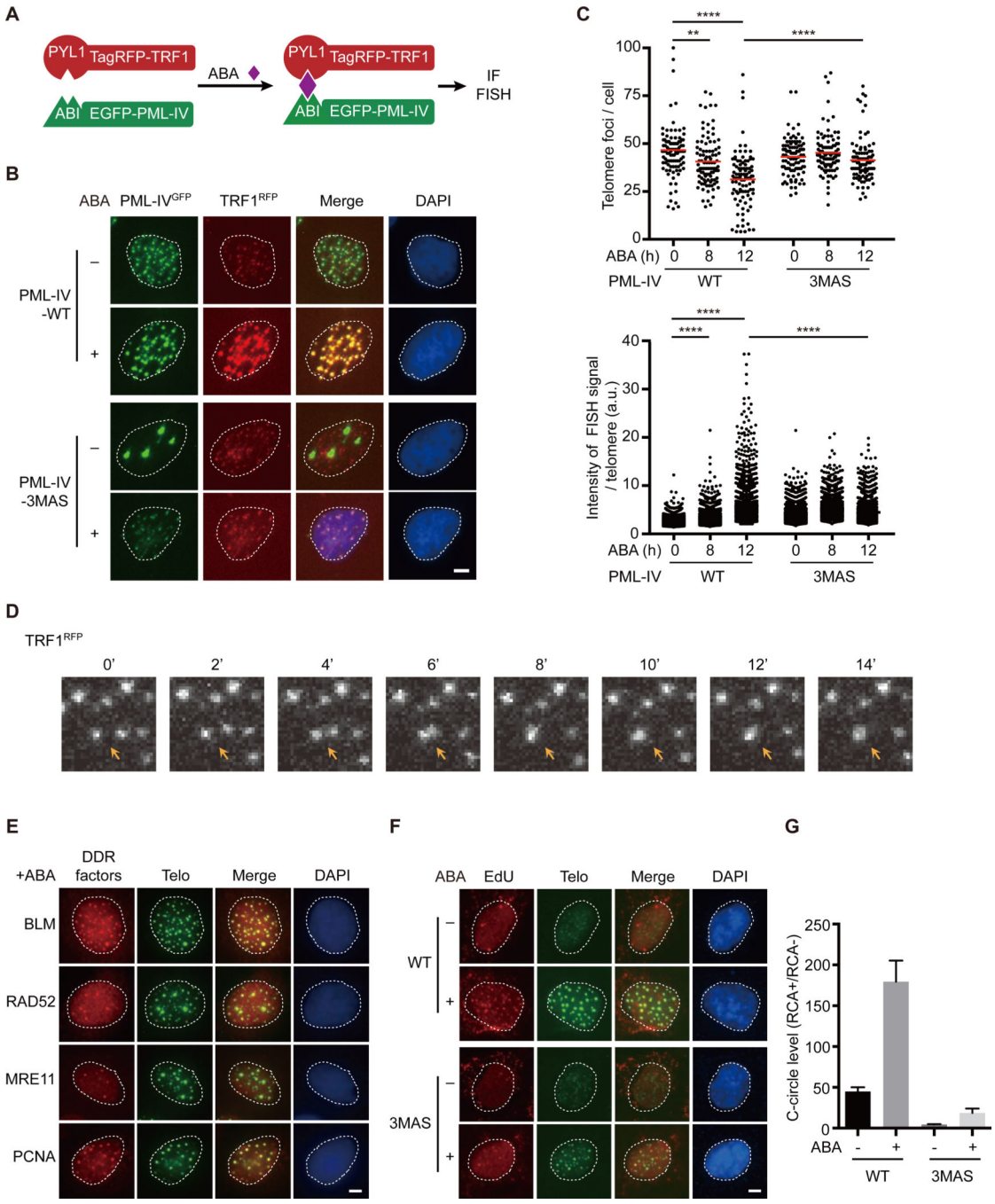

Figure 1. Tethering of PML-IV to telomeres induces APBs, telomere clustering, and telomere synthesis.

(A) A schematic of the ABA-induced tethering of PML-IV to telomeres. **(B)** U2OS cells expressing TRF1^{RFP} and PML-IV-WT^{GFP} or PML-IV-3MAS^{GFP} were treated with DMSO or ABA for 18 h. Fluorescence of PML-IV^{GFP} and RFP^{GFP} was directly analyzed. Scale bar: 5 μm. **(C)** U2OS cells expressing TRF1^{RFP} and PML-IV-WT^{GFP} or PML-IV-3MAS^{GFP} were exposed to ABA as indicated. Telomeres were detected by FISH, and the numbers of telomere foci (upper) in individual cells (n=100) and FISH intensity (lower) of individual

telomeres (n=2,000) were quantified. Red lines: mean numbers of telomere foci per cell. **p<0.001, ****p < 0.0001, determined by unpaired Student's t test. **(D)** Time-lapse imaging of a U2OS cell expressing $TRF1^{RFP}$ and PML-IV^{GFP} treated with ABA for 10 h. $TRF1^{RFP}$ was imaged every 2 min. The telomeres undergoing fusion were marked by yellow arrows. **(E)** U2OS cells expressing $TRF1^{RFP}$ and PML-IV-WT^{GFP} were exposed to ABA for 14 h. BLM, RAD52, MRE11 and PCNA were analyzed by IF, and telomeres were detected by FISH. Scale bar: 5 μm. **(F-G)** U2OS cells expressing $TRF1^{RFP}$ and PML-IV-WT^{GFP} or PML-IV-$3MAS^{GFP}$ were treated with DMSO or ABA for 18 h. In (F), cells were labeled with EdU for 1 h, and the EdU and telomeres in non-S phase cells were analyzed by IF and FISH, respectively. Scale bar: 5 μm. In (G), telomere DNA contents were determined by qPCR with or without rolling circle amplification (RCA) (Fig. S1J). The relative levels of C-circles were determined by the RCA+/RCA− ratio. Error bars, SD (n= 3).

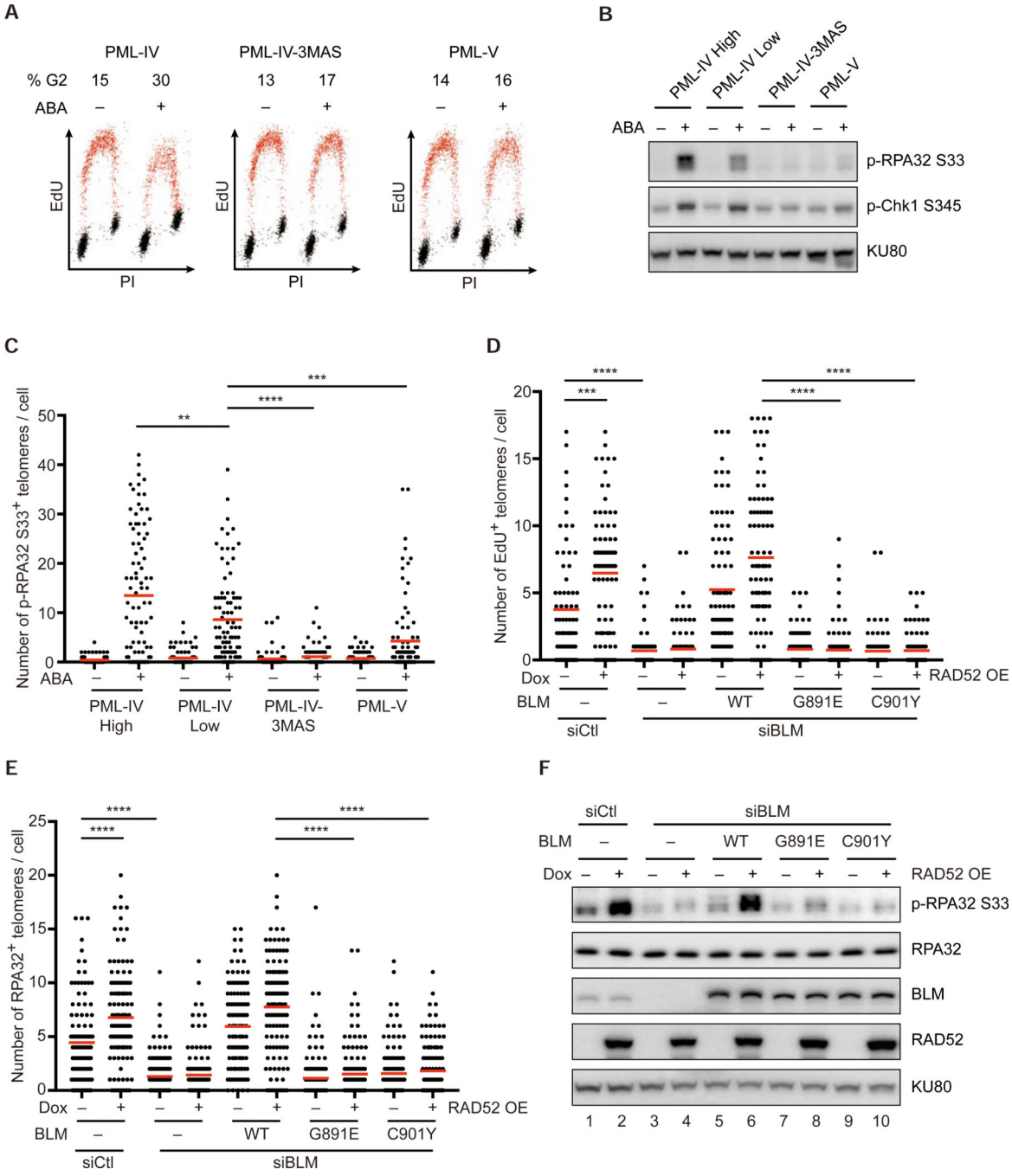

Figure 2. Enhanced ALT induces replication stress.

(A) U2OS cells expressing TRF1^{RFP} and PML-IV-WT^{GFP}, PML-IV-3MAS^{GFP}, or PML-V^{GFP} were treated with DMSO or ABA for 18 h, and then labeled with EdU for 0.5 h. Cell-cycle profiles were generated with EdU and propidium iodide (PI) signals. S-phase cells are colored in red. Three technical repetitions were performed. **(B-C)** U2OS cells expressing TRF1^{RFP} and the indicated PML variants were treated with DMSO or ABA. In (B), the indicated proteins were analyzed by western blot. In (C), the numbers of p-RPA32 S33^{+} telomeres in individual cells (n=92) were quantified. Red lines: mean numbers of p-RPA32

$S33^+$ telomeres per cell. **(D-F)** RAD52-inducible U2OS cells transfected with control or BLM siRNA were synchronized in G2 with CDK1i. Where indicated, cells were treated with doxycycline (Dox) to induce RAD52 overexpression (RAD52 OE), and infected with lentiviruses expressing siRNA-resistant BLM^{WT}, BLM^{G891E}, or BLM^{G901Y}. In (D), DNA synthesis at telomeres was detected by EdU labeling and telomere FISH. The numbers of EdU^+ telomeres in individual cells (n=85) were quantified. Red lines: mean numbers of EdU^+ telomeres per cell. Two biological repetitions were performed. In (E), the numbers of RPA^+ telomeres in individual cells (n=119) were quantified. Red lines: mean numbers of RPA^+ telomeres per cell. In (F), the indicated proteins were analyzed by western blot. In all relevant panels, $^{**}p<0.001$, $^{***}p<0.005$, $^{****}p < 0.0001$, determined by unpaired Student's t test.

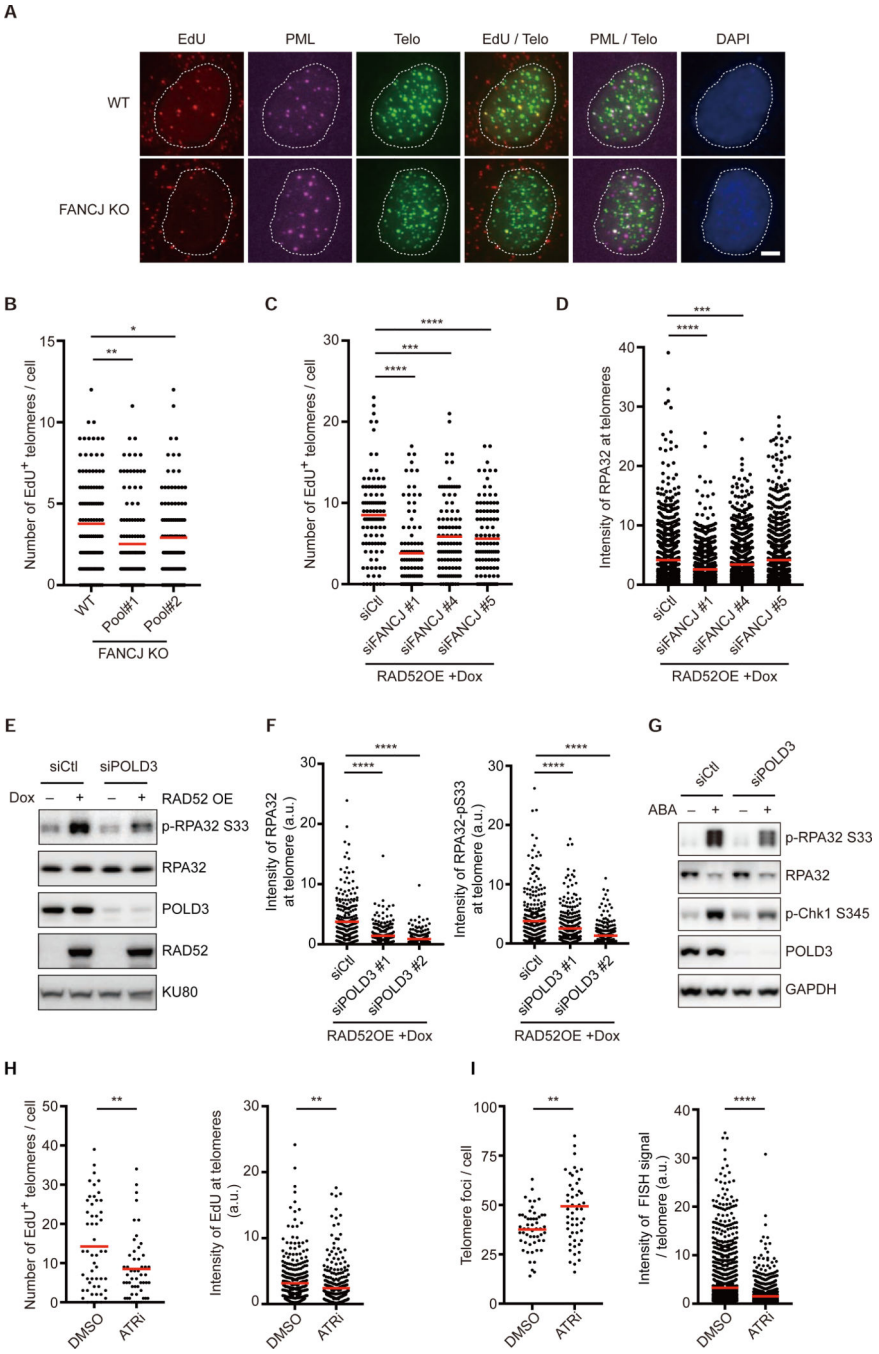

Figure 3. FANCJ and POLD3 contribute to ALT telomere synthesis and the associated replication stress.

(A-B) Wild-type (WT) and FANCJ KO U2OS cells were synchronized in G2 with CDK1i for 18 h, and then labeled with EdU for 1 h. In (A), EdU and PML were analyzed by IF and telomeres were detected by FISH. Scale bar: 5 μm. In (B), the numbers of EdU^+ telomeres in individual cells (n=194) were quantified. Red lines: mean numbers of EdU^+ telomeres per cell. **(C-D)** RAD52-inducible U2OS cells transfected with control or FANCJ siRNA were synchronized in G2 with CDK1i. In (C), the numbers of EdU^+ telomeres in individual cells (n=378) were quantified. Red lines: mean numbers of EdU^+ telomeres per cell. In (D), the

intensity of RPA32 at individual telomeres (n=1122) was quantified. Red lines: mean intensities of RPA32 at individual telomeres. **(E-F)** RAD52-inducible U2OS cells transfected with control or POLD3 siRNA were synchronized in G2 with CDK1i. In (E), the indicted proteins were analyzed by western blot. In (F), the intensity of RPA32 or p-RPA32 S33 at individual telomeres (n=278 for RPA32; n=316 for p-RPA32 S33) was quantified. Red lines: mean intensities of RPA32 or p-RPA32 S33 at individual telomeres. **(G)** U2OS cells expressing $TRF1^{RFP}$ and PML-IV^{GFP} were transfected with control or POLD3 siRNA, and then treated with DMSO or ABA for 18 h. **(H-I)** U2OS cells expressing $TRF1^{RFP}$ and PML-IV^{GFP} were treated by ABA together with DMSO or ATRi (10 μM VE-821) for 18 h and then labeled with EdU for 1 h. In (H), the number of EdU^+ telomeres in individual cells (left , n=52) and the intensity of EdU at individual telomeres (right, n=352) were quantified. Red lines: mean numbers of EdU^+ telomeres in individual cells (left) or mean intensities of EdU at individual telomeres (right). In (I), the number of telomere foci per cells (left, n=52) and the FISH intensity of individual telomeres (right, n=1,980) were quantified. Red lines: mean numbers of telomere foci per cells (left) or mean intensities of individual telomeres (right). Two biological repetitions were performed in the experiments in panels C, F, H, and I. In all relevant panels, *p<0.05, **p<0.001, ***p<0.005, ****p < 0.0001, determined by unpaired Student’s t test.

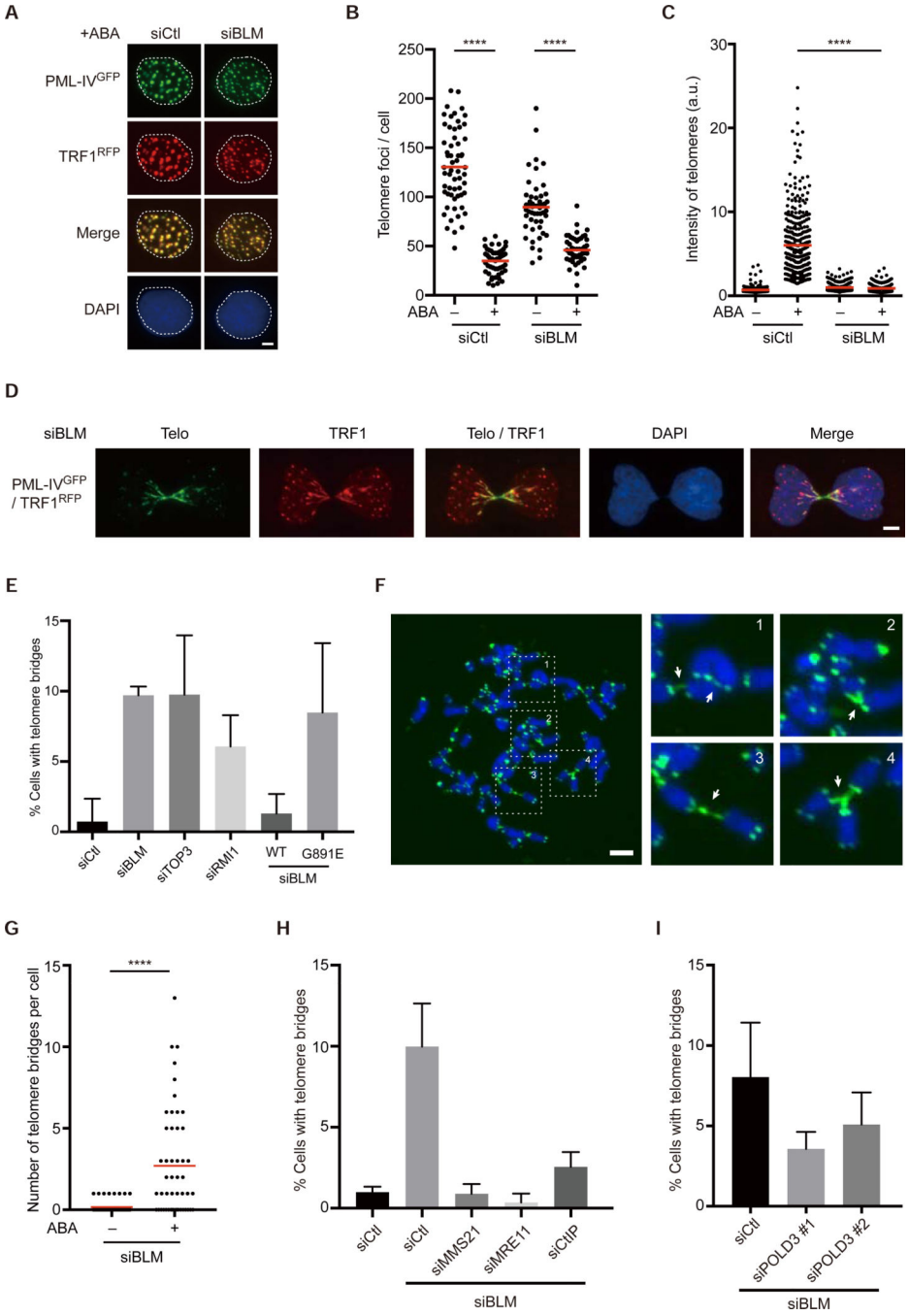

Figure 4. BLM drives ALT in APBs by resolving BIR intermediates.

(A) U2OS cells expressing PML-IV^{GFP} and TRF1^{RFP} were transfected with control or BLM siRNA, and then treated with ABA for 18 h. PML bodies and telomeres were detected by the fluorescence of PML-IV^{GFP} and TRF1^{RFP}. Scale bar: 5 μm. **(B-C)** U2OS cells expressing PML-IV^{GFP} and TRF1^{RFP} were transfected with control or BLM siRNA, and then treated with DMSO or ABA for 18 h. In (B), the numbers of telomere foci in individual cells (n=50) were quantified. In (C), the FISH intensity of individual telomeres (n=345) was quantified. Red lines: mean numbers of telomere foci per cell (B) or mean intensities of individual

telomeres (C). **(D)** U2OS cells expressing PML-IV^{GFP} and TRF1^{RFP} were transfected with BLM siRNA, and then treated with ABA for 18 h. TRF1^{RFP} and telomeres were detected by IF and FISH, respectively. Scale bar: 5 μm. **(E)** U2OS cells expressing PML-IV^{GFP} and TRF1^{RFP} were transfected with control, BLM, TOP3, or RMI1 siRNA. Where indicated, cells were infected with lentiviruses expressing siRNA-resistant BLM^{WT} or BLM^{G891E}. Cells were treated with ABA for 18 h and quantified for telomere bridges based on TRF1^{RFP} signals. The mean fractions of cells with telomere bridges were determined from 5 sets of randomly selected images. Error bar, SD. **(F)** U2OS cells expressing PML-IV^{GFP} and TRF1^{RFP} were transfected with BLM siRNA, and then treated with ABA for 12 h and colcemid for another 4 h. Metaphase chromosome spreads were prepared, and telomeres were detected by FISH. Scale bar: 5 μm. **(G)** U2OS cells expressing PML-IV^{GFP} and TRF1^{RFP} were transfected with BLM siRNA, and then treated with DMSO or ABA for 12 h and colcemid for another 4 h. The numbers of telomere bridges in individual metaphase spreads (n=50) were quantified. Red lines: mean numbers of telomere bridges per cell. **(H-I)** U2OS cells expressing PML-IV^{GFP} and TRF1^{RFP} were transfected with control or BLM siRNA. Where indicated, MMS21 (H), MRE11 (H), CtIP (H), or POLD3 (I) siRNA was transfected with BLM siRNA. Cells were treated with ABA for 18 h and quantified for telomere bridges as in (E). The mean fractions of cells with telomere bridges were determined from 6 (H) or 10 (I) sets of randomly selected images. Error bar, SD. In all relevant panels, ****$p < 0.0001$, determined by unpaired Student's t test.

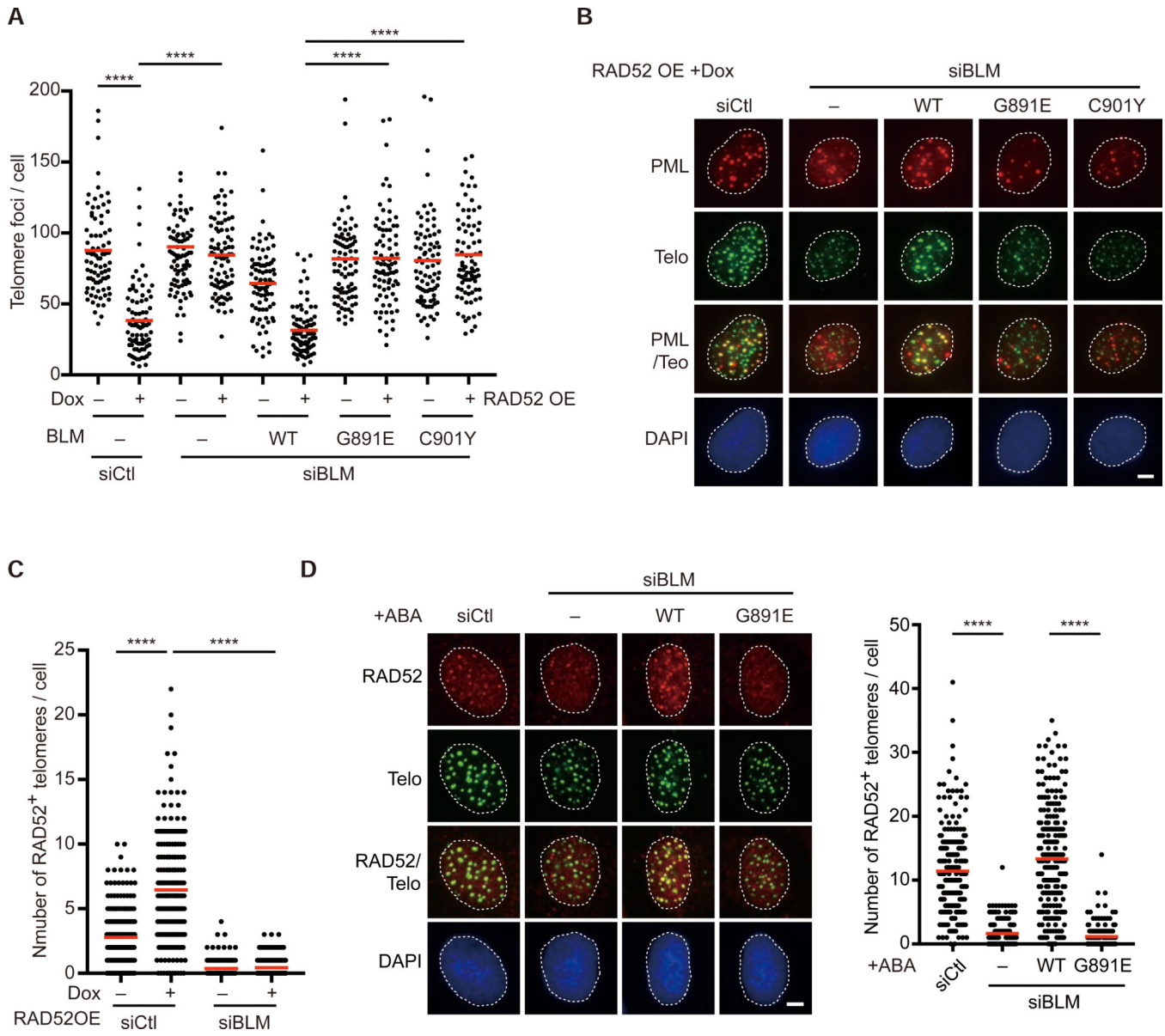

Figure 5. BLM mediates RAD52-driven ALT activity and promotes RAD52 accumulation in APBs.

(A-B) RAD52-inducible U2OS cells were transfected with control or BLM siRNA, and then synchronized in G2 with CDK1i. Where indicated, cells were treated with Dox to induce RAD53 OE and infected with lentiviruses expressing siRNA-resistant BLM^{WT}, BLM^{G891E}, or BLM^{G901Y}. In (A), the numbers of telomere foci in individual cells (n=85) were quantified. Red lines: mean numbers of telomere foci number per cell. In (B), PML and telomeres in representative cells are shown. **(C)** RAD52-induible U2OS cells transfected with control or BLM siRNA were synchronized in G2 with CDK1i. The numbers of $RAD52^+$ telomeres in individual cells (n=200) were quantified. Red lines: mean numbers of $RAD52^+$ telomeres per cell. Two biological repetitions were performed. **(D)** U2OS cells expressing PML-IV^{GFP} and $TRF1^{RFP}$ were transfected with control or BLM siRNA, and treated with ABA for 14 h. Where indicated, cells were infected with lentiviruses expressing

siRNA-resistant BLM^{WT} or BLM^{G891E}. Left panel: RAD52 and telomeres in representative cells are shown. Right panel: the numbers of $RAD52^{+}$ telomeres in individual cells (n=213) were quantified. Red lines: mean numbers of $RAD52^{+}$ telomeres per cell. In all relevant panels, ****$p < 0.0001$, determined by unpaired Student's t test. Scale bar: 5 μm.

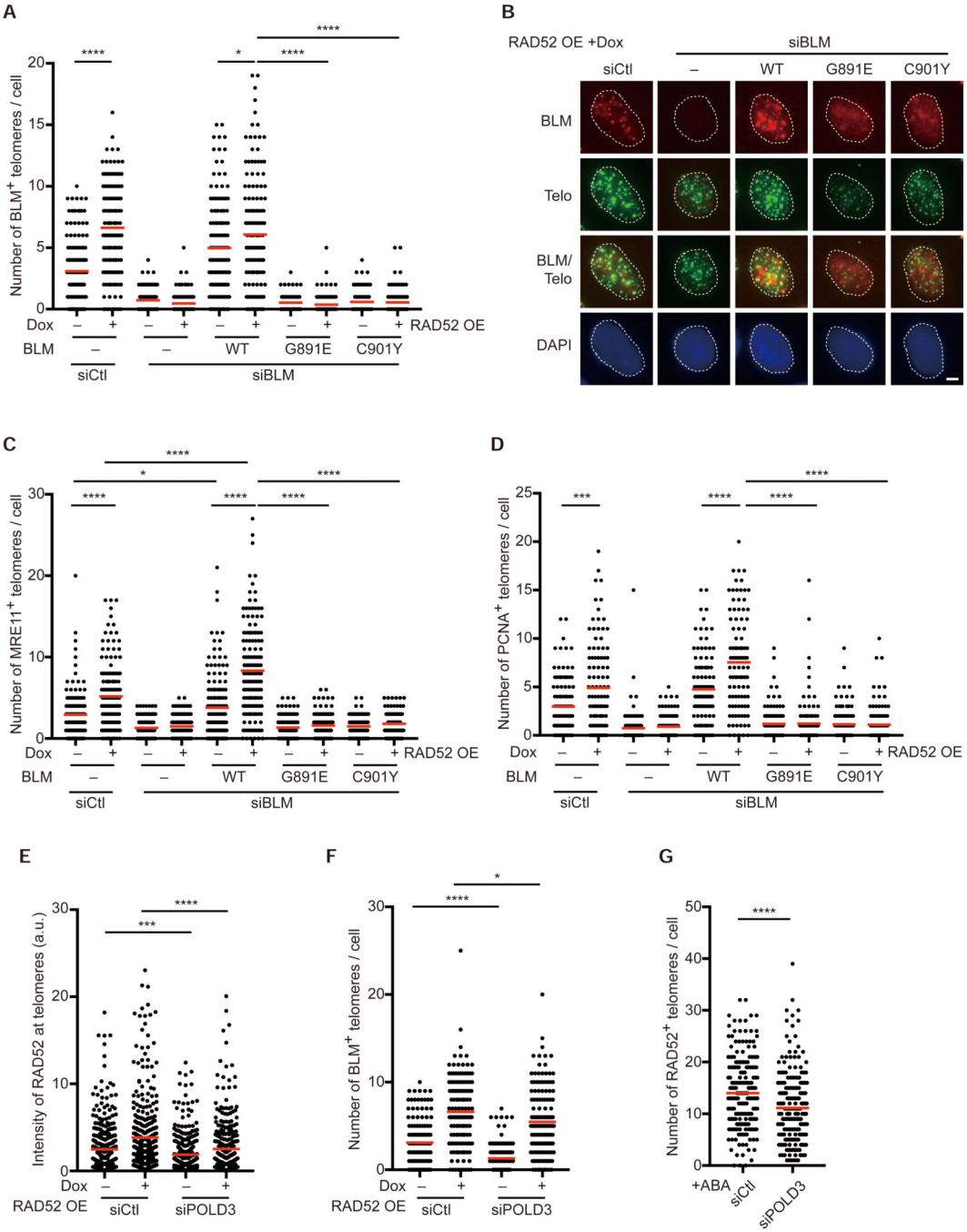

Figure 6. BIR drives a feedforward loop to promote accumulation of DDR proteins in APBs.

(A-B) RAD52-inducible U2OS cells transfected with control or BLM siRNA were synchronized in G2 with CDK1i. Where indicated, cells were treated with Dox to induce RAD52 OE and infected with lentiviruses expressing siRNA-resistant BLM^{WT}, BLM^{G891E}, or BLM^{G901Y}. In (A), the numbers of BLM^{+} telomeres in individual cells (n=140) were quantified. Red lines: mean numbers of BLM^{+} telomeres per cell. In (B), BLM and telomeres in representative cells are shown. Scale bar: 5 μm. (**C-D**) RAD52-inducible U2OS cells were processed as in (A). In (C), the numbers of $MRE11^{+}$ telomeres in individual cells

(n=148) were quantified. In (D), the numbers of $PCNA^{+}$ telomeres in individual cells (n=103) were quantified. Red lines: mean numbers of $MRE11^{+}$ (C) or $PNCA^{+}$ (D) telomeres per cell. **(E-F)** RAD52-induicle U2OS cells transfected with control or POLD3 siRNA were synchronized in G2 with CDK1i. In (E), the intensity of RAD52 at individual telomeres (n=384) was quantified. In (F), the numbers of BLM^{+} telomeres in individual cells (n=140) were quantified. Red lines: mean intensities of RAD52 at individual telomeres (E) or mean numbers of BLM^{+} telomeres per cell (F). **(G)** U2OS cells expressing PML-IV^{GFP} and $TRF1^{RFP}$ were transfected with control or POLD3 siRNA, and then treated with ABA for 14 h. The numbers of $RAD52^{+}$ telomeres in individual cells (n=213) were quantified. Red lines: mean numbers of $RAD52^{+}$ telomeres per cell. In all relevant panels, *p<0.05, **p<0.001, ***p<0.005, ****p < 0.0001, determined by unpaired Student's t test.

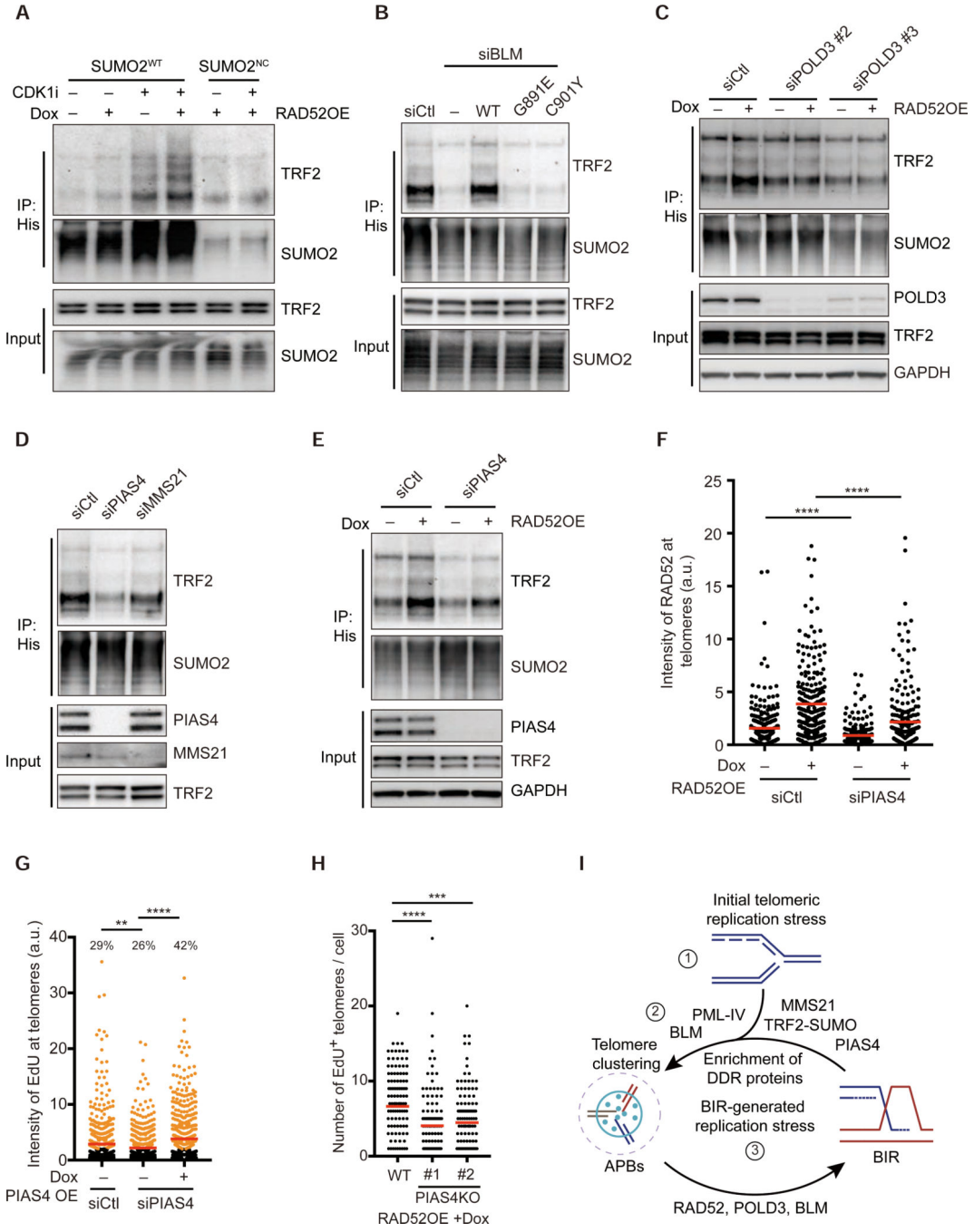

Figure 7. PIAS4 promotes TRF2 SUMOylation and mediates the BIR-driven feedforward loop.

(A) RAD52-inducible U2OS cells expressing 10xHis-SUMO2^{WT} or 10xHis-SUMO2^{NC} were treated with CDK1i and/or Dox as indicated. SUMOylated proteins were captured with Ni-NTA beads under a denaturing condition. Levels of TRF2 and SUMO2 in inputs and His pulldowns were analyzed by western blot. **(B)** U2OS cells expressing 10xHis-SUMO2^{WT} were transfected with control or BLM siRNA, and then synchronized in G2 with CDK1i. Where indicated, cells were infected with lentiviruses expressing siRNA-resistant BLM^{WT}, BLM^{G891E}, or BLM^{G901Y}. **(C-E)** RAD52-inducible U2OS cells expressing 10xHis-

SUMO2^{WT} were transfected with control, POLD3 (C), MMS21 (D), and PIAS4 (C-D) siRNAs, and then synchronized in G2 with CDK1i. **(F)** RAD52-inducible U2OS cells transfected with control or PIAS4 siRNA were synchronized in G2 with CDK1i. The intensity of RAD52 at individual telomeres (n=246) was quantified. Red lines: mean intensities of RAD52 at individual telomeres. **(G)** U2OS cells that inducibly express siRNA-resistant PIAS4 were transfected with control or PIAS4 siRNA and synchronized in G2 with CDK1i. Cells were treated with Dox to induce PIAS4 expression. The intensity of EdU at individual telomeres (n=553) were quantified. Telomeres with significant EdU signals are colored in orange. The percentage of all EdU$^+$ telomeres is indicated above each sample. Red lines: mean EdU intensities at telomeres. Two biological repetitions were performed. **(H)** RAD52-inducible WT and PIAS4 KO U2OS cells (two clones) were synchronized in G2 with CDK1i. The numbers of EdU$^+$ telomeres in individual cells (n=121) were quantified. Red lines: mean numbers of EdU$^+$ telomeres per cell. **(I)** A model illustrating the key events driving activation of the ALT pathway. In all relevant panels, **p<0.001, ***p<0.005, ****p < 0.0001, determined by unpaired Student's t test.

KEY RESOURCES TABLE

REAGENT or RESOURCE	SOURCE	IDENTIFIER
Antibodies		
Biotin	Abcam	ab53494
BLM	Bethyl	A300-110A
Chk1pS345	Cell Signaling Technology	2348
FANCJ	Sigma	B1310
GAPDH	Santa Cruz	sc-32233
KU80	NeoMarker	MS-285-P1
MMS21	Bethyl	A304-126A
MRE11	Genetex	GTX70212
PCNA	Abcam	Ab18197
PIAS4	Cell Signaling	4392
PML	Abcam	ab96051
PML	Santa Cruz	sc-5621
POLD3	Bethyl	A301-244A
RAD52	Santa Cruz	sc-8350
RAD52	Abcam	ab124971
RPA32	Thermo Fisher	MA1-26418
RPA32pS33	Bethyl	A300-246A
SP100	Abcam	ab167605
SUMO2/3	MBL	M114-3
TRF2	Cell Signaling Technology	2645
TRF2	Novus Biology	NB110-57130
Chemicals, Peptides, and Recombination Proteins		
(+)-Abscisic Acid	Cayman chemical	21293-29-8
20x SSC	Thermo Fischer	AM9763
ATR inhibitor (VE-821)	Selleckchem	S8007
ATM inhibitor (KU55933)	Selleckchem	S1092
Azide-PEG3-Biotin	Sigma	762024-10MG
BSA	NEB	B9000S
CDKi (RO-3306)	Selleckchem	S7747
Click-iT™ EdU Alexa Fluor™ 488 Imaging Kit	Thermo Fischer	C10337
Dextran Sulfate sodium	Sigma	D8906-10G
dNTP Set(100 mM)	Thermo Fischer	10297018
Formamide	Sigma	47671-1L-F
Ni-NTA beads	Invitrogen	R90115
phi29 DNA Polymerase	NEB	M0269L
PureLink™ Genomic DNA Mini Kit	Thermo Fischer	K182002

REAGENT or RESOURCE	SOURCE	IDENTIFIER
TelC-FITC	PNA Bio	F1009
Experimental Models: Cell Lines		
RPE-1	ATCC	N/A
U-251MG	ATCC	N/A
U2OS	ATCC	N/A
U2OS TRF1^{RFP} PML-IV-WT^{GFP}	This paper	N/A
U2OS TRF1^{RFP} PML-IV-3MAS^{GFP}	This paper	N/A
U2OS RAD52OE:	This paper	N/A
U2OS PIAS4OE:	This paper	N/A
U2OS FANCJ KO #1 and #2	This paper	N/A
U2OS PIAS4 KO #1 and #2	This paper	N/A
Oligonucleotides		
See Table S1 for siRNAs	This paper	N/A
See Table S2 for primers for C circle	This paper	N/A
Recombinant DNA		
pLenti PGK ABI-EGFP-PMLIV-WT	This paper	N/A
pLenti PGK ABI-EGFP-PMLIV-3MAS	This paper	N/A
pLenti PGK PYL1-TagRFP-TRF1	This paper	N/A
pInducer20-RAD52-HA	Zhang et al., 2019	N/A
pHAGE-EF1a-3*HA-BLM-siR-WT	This paper	N/A
pHAGE-EF1a-3*HA-BLM-siR-G891E	This paper	N/A
pHAGE-EF1a-3*HA-BLM-siR-C901Y	This paper	N/A
pInducer20-PIAS4-siR-HA	This paper	N/A
pInducer20-MMS21-siR-HA	This paper	N/A
Software and Algorithms		
Image Lab	BioRad	http://www.bio-rad.com/enus/product/image-labsoftware
NIS element viewer	Nikon	https://www.nikoninstruments.com/Products/Software/NIS-Elements-AdvancedResearch/NIS-Elements-Viewer
GraphPad Prism 7	GraphPad Software, Inc.	https://www.graphpad.com/scientific-software/prism/
Image J	NIH	https://imagej.nih.gov/ij/
FociLab 2.0	Li-Lin Du's lab, National Institute of Biological Sciences, Beijing	N/A